An extracellular redox signal triggers calcium release and impacts the asexual development of *Toxoplasma gondii*

Eduardo Alves[1], Henry J. Benns[1,2], Lilian Magnus[1], Caia Dominicus[3], Tamás Dobai[1], Joshua Blight[1], Ceire J. Wincott[1], Matthew A. Child[1]*

[1]Department of Life Sciences, Imperial College London, Exhibition Road, South Kensington, London, SW7 2AZ, UK.

[2]Department of Chemistry, Imperial College London, 82 Wood Lane, White City, London, W12 0BZ, UK.

[3]Signaling in Apicomplexan Parasites Laboratory, The Francis Crick Institute, 1 Midland Road, NW1 1AT, London, UK

*To whom correspondence should be addressed: m.child@imperial.ac.uk

Abstract

The ability of an organism to sense and respond to environmental redox fluctuations relies on a signaling network that is incompletely understood in apicomplexan parasites such as *Toxoplasma gondii*. The impact of changes in redox upon the development of this intracellular parasite is not known. Here, we provide a revised collection of 58 genes containing domains related to canonical antioxidant function, with their encoded proteins widely dispersed throughout different cellular compartments. We demonstrate that addition of exogenous H_2O_2 to human fibroblasts infected with *T. gondii* triggers a Ca^{2+} flux in the cytosol of intracellular parasites that can induce egress. In line with existing models, egress triggered by exogenous H_2O_2 is reliant upon both Calcium-Dependent Protein Kinase 3 and diacylglycerol kinases. Finally, we show that the overexpression a glutaredoxin-roGFP2 redox sensor fusion protein in the parasitophorous vacuole severely impacts parasite replication. These data highlight the rich redox network that exists in *T. gondii*, evidencing a link between extracellular redox and intracellular Ca^{2+} signaling that can culminate in parasite egress. Our findings also indicate that the redox potential of the intracellular environment contributes to normal parasite growth. Combined, our findings highlight the important role of redox as an unexplored regulator of parasite biology.

Introduction

Toxoplasma gondii is a single-cell obligate intracellular parasite from the Apicomplexa phylum that can infect any warm-blooded animal. Its seroprevalence is estimated at more than one-third of the human population[1, 2]. Within the host, the asexual lifecycle of *T. gondii* exists as two distinct stages: rapidly proliferating tachyzoites that characterize the acute infection, and slower replicating encysted bradyzoites that are associated with chronic infection[3, 4]. While infections are usually benign, in immunocompromised patients and foetuses[5, 6] the lytic tachyzoite lifecycle is responsible for severe clinical pathology. During a lytic cycle, tachyzoites attach onto and actively penetrate host cells, forming a permissive replication niche called the parasitophorous vacuole (PV). Parasites then replicate by endodyogeny[7] until they eventually egress from the host cell, leading to its lytic destruction. The interconversion of virulent tachyzoites with persistent encysted bradyzoites is influenced by host immune pressure and is key to understanding disease recrudescence[8]. The ability of *T. gondii* to infect diverse host species relates to its remarkable capacity to resist host defences, efficiently recognize and quickly respond to myriad environmental clues. Among biological signal cascades activated by external clues, Ca^{2+} signaling is the most notable and best studied in *T. gondii* (reviewed in [9]). Ca^{2+} is a ubiquitous signaling molecule with a vital role in tachyzoite host-cell invasion[10, 11], motility[12] and egress[13] through activation of effector proteins such as the plant like Ca^{2+}-dependent Protein Kinase 1 (CDPK1)[14, 15] and CDPK3[16]. Alongside Ca^{2+}, other intracellular signaling molecules are known to play important roles in the tachyzoite lytic cycle. These include phosphatidic acid (PA)[17], and the activation of protein kinase G by cyclic guanidine monophosphate (cGMP)[18].

Contrasting with Ca^{2+}, the study of reactive oxygen species (ROS) as signaling molecules is incipient in the Apicomplexa. Hydrogen peroxide (H_2O_2) is a neutral ROS molecule with an ability to cross membranes[19], and its roles in signaling are diverse. These include its interaction with glutathione (GSH), and the oxidation of cysteine residues leading to allosteric changes in a variety of proteins such as phosphatases, transcription factors and ion channels[20]. Typically, the oxidation of redox-sensitive cysteines is a reversible process catalysed by enzymes that use GSH or nicotinamide adenine dinucleotide phosphatase (NADPH)[21-24] as redox cofactors. Most studies of H_2O_2 and *T.*

gondii tachyzoites have focused on the ability of host cells to use the damaging oxidative properties of ROS as a component of innate defence, and strategies employed by tachyzoites to overcome this defence[25-29].

A *T. gondii* orthologue of the H_2O_2-detoxifying enzyme catalase is expressed in the parasite cytosol, and confers protection against host oxidative stress[26, 30]. In 2004 Ding *et al.,* [26] compiled a group of 14 genes related to the *T. gondii* antioxidant system. These typically localized to the parasite cytosol and mitochondria, and were assigned to one of five major redox system classifications: (1) metabolic genes (e.g. superoxide-dismutase and catalase); (2) thioredoxins (Trxs, proteins that promote cysteine thiol-disulfide exchange); (3) Protein Disulfide Isomerases (PDIs, proteins that disrupt or form cysteine disulfide bonds to assist protein folding); (4) glutaredoxin-glutathione (Grx-GSH, small proteins that use GSH as a cofactor for thiol-disulfide exchange) and (5) peroxiredoxins (Prxs, enzymes that detoxify hydroperoxides like H_2O_2 and organic hydroperoxides).

Expanding this broad description of the parasite's antioxidant system, other studies have tested the association of redox with *T. gondii* signaling and cell cycle regulation. Exogenous treatment of intracellular parasites with the reducing agent dithiothreitol (DTT) triggers Ca^{2+} mobilization and parasite egress[31]. This egress response was triggered by the depletion of host-cell ATP resulting from the activity of an exported parasite ATPase[32]. In a separate study, the oxidation-sensitive protein *Tg*DJ-1 was found to associate with CDPK1 and promote microneme secretion in *T. gondii*[33]. More recently, oxidative stress (generated by sodium arsenite) has been shown to trigger tachyzoite differentiation into bradyzoites following phosphorylation of *T. gondii* eIF2α (TgIF2α) by the translation initiation factor kinase *Tg*IF2K-B[34]. Together, these data suggest that *T. gondii* modulates biological processes in response to changes in redox homeostasis.

Here, we use an *in silico* approach to establish a compendium of redox-associated genes and provide an updated view of these genes in *T. gondii*. We then investigate the impact of H_2O_2 upon parasite biology, demonstrating that a H_2O_2 signal outside the boundaries of the infected host cell can be received and interpreted deep within the cytosol of intracellular parasites. We find that exogenous treatment of H_2O_2 triggers mobilization of Ca^{2+} culminating in CDPK3-dependent egress. Finally, we use a genetically encoded redox reporter to dissect redox oscillations prior to egress. Unexpectedly,

we discover that overexpression of the active catalytic domain of a human Grx in the parasite's cytosol or PV delays parasite asexual replication. Our results corroborate the existence of a rich variety of antioxidant proteins located in multiples cellular compartments and highlight importance of redox in the basic biology of *T. gondii*.

Results

An updated compendium of T. gondii redox-associated genes

We initially sought to update our understanding of the antioxidant response and redox-signaling network in *T. gondii*. We mined gene sequence and annotation information, as well as proteomic datasets present on ToxoDB[35] to update the list of 14 redox associated genes previously summarised by Ding *et al.,* 2004[26]. Our bioinformatic approach screened for genes containing at least one functional domain of the major redox signaling groups (Trxs, PDIs, Grx-GSHs and Prxs). We identified a total of 58 redox-associated genes (Supplemental material table S1), including 26 Trxs, 16 GRX-GSHs, six PDIs, six Prxs, and four metabolic genes (including three distinct superoxide dismutases and one catalase). With the exception of the metabolic genes[26, 30, 36, 37], the majority of genes representing the other redox signaling groups remain uncharacterized. For an improved view of the subcellular distribution of these gene products, we extracted their primary localisation from the recently published hyperLOPIT dataset[38] (Figure 1 – table supplement 1). This indicated a broad distribution of these proteins throughout the cell and suggested the existence of spatially distinct mechanisms of redox regulation for different subcellular compartments.

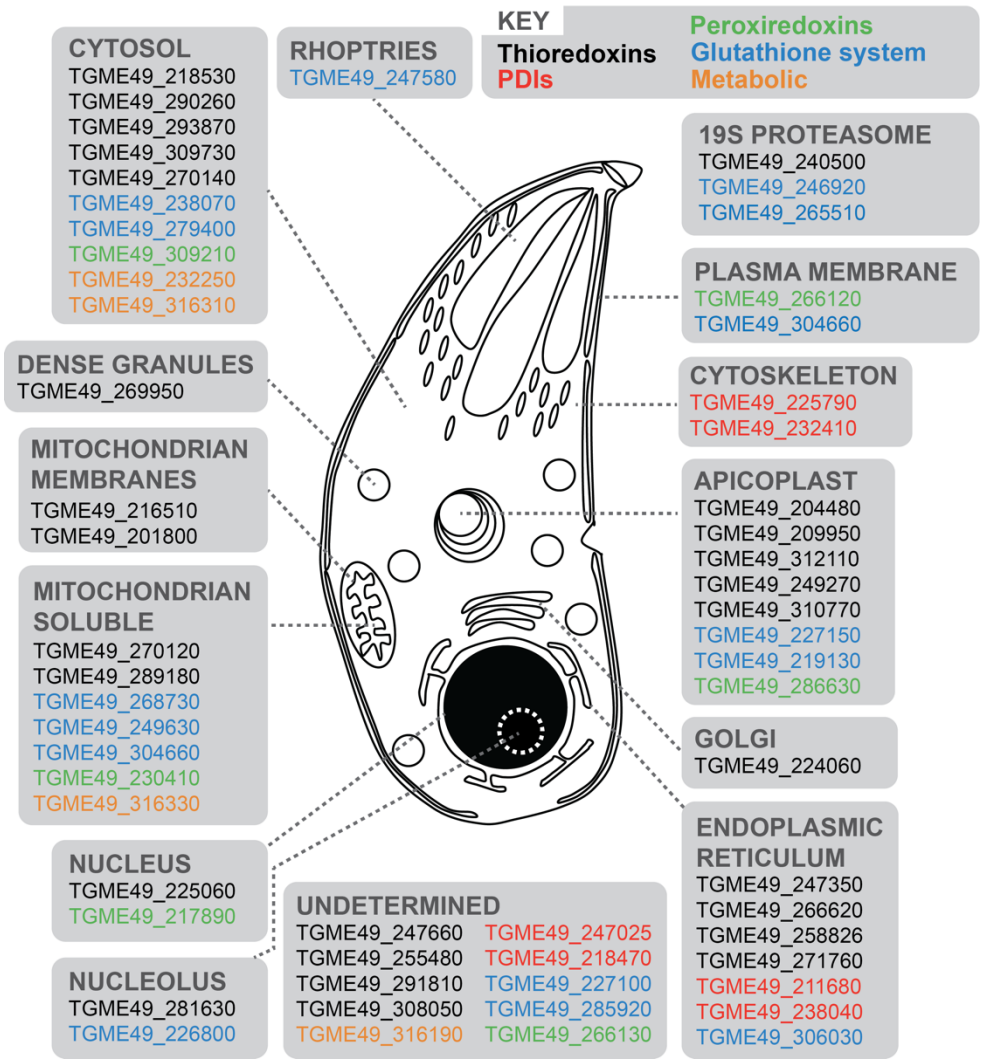

Figure 1: Schematic representation of a *T. gondii* tachyzoite displaying 58 redox-associated genes, and their primary protein location as determined by HyperLOPIT[38]. Gene ID accession numbers are provided, and genes categorized into five groups: black (Trxs); red (PDIs); green (Prxs); blue (Grx-GSHs) and orange (metabolic genes). Further details are provided in Supplement table S1.

Extracellular hydrogen peroxide induces cytosolic Ca^{2+} flux in intracellular tachyzoites

In other eukaryotic systems there are clear associations between calcium and redox signaling. For example, oxidation of cysteines on the ryanodine receptor stimulates calcium release from intracellular compartments[39, 40]. To investigate if a similar overlap exists between these two signaling networks in *T. gondii*, we tested the ability of H_2O_2 to trigger a Ca^{2+} response in tachyzoites within a host cell. We generated a Type 1 parasite (RH strain) expressing the Ca^{2+} sensor protein jRCamP1b[41] fused to GFP via the T2A peptide for bicistronic protein expression (referred to as RH-GFP-T2A-jRCaMP1b). The ratio of these two distinct fluorescent proteins provided an elegant tool to distinguish changes in fluorescence due to cell movement from the Ca^{2+} signal (Figure 2 – figure supplement 1A and B). Upon exogenous addition of 100 µM H_2O_2 we observed a distinct spike in the intracellular Ca^{2+} reporter signal (Figure 2A – videos supplement 1, 2 and 3). To determine whether the oxidative properties of H_2O_2 are responsible for triggering parasite Ca^{2+} release, we repeated the experiment in the presence of the antioxidant α-tocopherol (Figure 2B). Pre-treatment of infected host cell monolayers with 50 µM α-tocopherol abolished H_2O_2-stimulated Ca^{2+} release in intracellular parasites. The addition of the Ca^{2+} ionophore A23187 caused an intense Ca^{2+} signal spike in the parasite cytosol in both the presence and absence α-tocopherol (Figure 2A and 2B, respectively), suggesting that the presence of the antioxidant does not interfere with Ca^{2+} stores in intracellular parasites. Vehicle solvent for H_2O_2 (water) and for A231877 (DMSO) did not trigger Ca^{2+} mobilisation (Figure 2 – figure supplement 1C and D, respectively).

We compared the magnitude of the Ca^{2+} signal increase following H_2O_2 treatment with the increase triggered by A23187, a small molecule known to induce parasite egress by Ca^{2+}-dependent mechanisms[42] (Figure 2C). H_2O_2 induced an overall Ca^{2+} signal increase of 35% ± 1.7. This was lower than the Ca^{2+} signal increase observed when parasites were treated with A23187 alone (140 ± 4.3), or A23187 on cells pre-treated with 100 µM H_2O_2 (61% ± 0.9). Within restricted timeframe of this experiment (10 minutes), a single egress event was observed for cells treated with 100 µM H_2O_2 (Figure 2C – video supplement 2). Observation of egress induced by H_2O_2 was more frequent when host cells were infected with a high multiplicity of infection (MOI = 5) (Figure 2 – video supplement 3). We also measured the magnitude of Ca^{2+} signal increase induced by H_2O_2 in Δ*CDPK3* parasites

(Figure 2D). The magnitude of the Ca^{2+} signal induced by H_2O_2 in RH-GFP-T2A-jRCaMP1bΔ*CDPK3* was lower (18.1% ± 4.3) compared to RH-GFP-T2A-jRCaMP1b (32.5% ± 1.1). This could reflect previously observed differences in the resting Ca^{2+} levels of these lines[43]. Together, these data suggest that tachyzoites within the PV can perceive and respond to oxidation events initiated outside the host cell.

Hydrogen peroxide induces parasite egress in a mechanism dependent on CDPK3

Calcium flux accompanies natural egress[44], and calcium ionophores are well-characterized inducers of egress[13]. To better investigate the potential of H_2O_2 to induce parasite egress, we analysed populations of infected host cells by flow cytometry. The GFP signal from parasites expressing the Ca^{2+} sensor and particle size were used to distinguish infected host cells from free tachyzoites (Figure 2 – figure supplement 2A). We tested whether treatment of infected host cells with different concentrations of H_2O_2 could increase the proportion of free tachyzoites. Incubation of infected host cells with H_2O_2 resulted in a dose-dependent increase in the number of free tachyzoites (Figure 2E). We sought to understand how the H_2O_2 stimulated egress integrates into our current molecular understanding of this process. The small molecule R59022 is an inhibitor of diacylglycerol kinase[45] that inhibits egress by disrupting the formation of phosphatidic acid[17]. For all concentration tested, treatment of cells with H_2O_2 resulted in a pharmacological rescue of R59022 egress inhibition. However in the presence of R59022, H_2O_2 did not stimulate egress above the baseline value. This could relate to the discrete points of activity for the two targets of R59022: diacylglycerol kinase 1 and 2[46] relative to where the H_2O_2 effect feeds into the system. The stimulation of egress by H_2O_2 was abolished in Δ*CDPK3* parasites (Figure 2F), demonstrating a dependency upon this kinase similar to other egress agonists such as A231287. The incubation of non-infected HFFs with different concentrations of H_2O_2 did not alter the proportion of events in this population (Figure 2 – figure supplement 2B), confirming that the concentrations of H_2O_2 used in this protocol did not lyse the host cells.

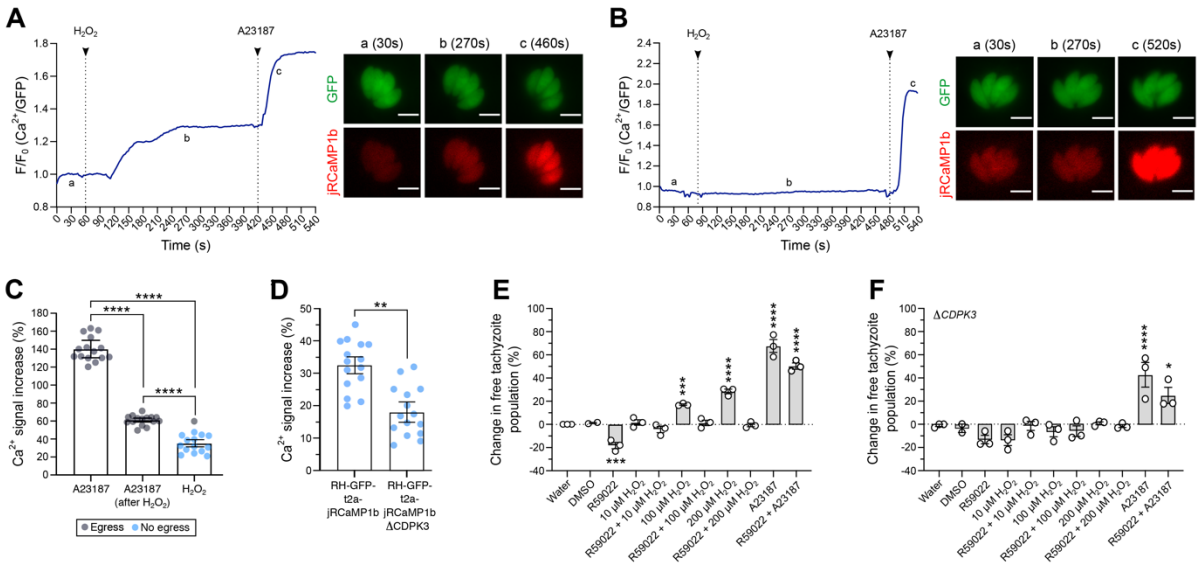

Figure 2: H_2O_2 induces Ca^{2+} release in intracellular parasites and triggers CDPK3-dependent egress. (**A**) Representative trace of 100 µM H_2O_2 induction of Ca^{2+} flux in intracellular RH-GFP-T2A-jRCaMP1b parasites. a – c: widefield microscopy images depicting changes in parasite fluorescence signal intensity for both GFP and the Ca^{2+} sensor at baseline (a at 30s), the peak of Ca^{2+} after H_2O_2 addition (b at 270s), and peak of Ca^{2+} after 1 µM A23187 addition (c at 460s). Data are representative of 27 infected vacuoles from four independent experiments. (**B**) Representative trace of 100 µM H_2O_2 induction of Ca^{2+} flux following pre-treatment of infected host cells with 50 µM α-tocopherol. a: baseline at 30s, b: trace after H_2O_2 addition at 270s and c: peak of Ca^{2+} triggered by A23187 at 520s. Data are representative of 14 infected vacuoles from three independent experiments. For (**A**) and (**B**): black arrows indicate the time of compound addition. Scale bar: 5 µM. (**C**) Intensity of parasite Ca^{2+} signal increase in RH-GFP-T2A-jRCaMP1b parasites (expressed as a percentage over baseline) following addition of: 1 µM A23187 alone, 1 µM of A23187 following 100 µM H_2O_2 pre-treatment, and 100 µM H_2O_2 alone. Gray dots indicate vacuole data points where parasite egress was observed during the measurement period, blue dots represent vacuoles where egress was not observed. (**D**) Intensity of parasite Ca^{2+} signal increase (%) over the baseline upon addition of 100 µM H_2O_2 in RH-GFP-T2A-jRCaMP1b *versus* RH-GFP-T2A-jRCaMP1bΔ*CDPK3* parasites. For (**C**) and (**D**): histograms present data mean ±SEM of three independent experiments (five vacuoles measured in each experiment), with individual vacuole data points also shown. (**E**) and (**F**): Egress assay measuring tachyzoite release after compound treatment in RH-GFP-T2A-jRCaMP1b and RH-GFP-T2A-jRCaMP1bΔ*CDPK3*, respectively. Data represent the mean ±SEM of three independent experiments (except for DMSO that has two independent experiments), with six technical replicates for each. All data were normalised to the water control. Significance was calculated using one-way Anova, Bonferroni's multiple comparisons test. P values: *< 0.05; **< 0.01, ***< 0.001 and ****< 0.0001.

Intracellular parasites expressing GRX1-roGFP2 sensor perceive oxidation induced by H_2O_2

After confirming that exogenous addition of H_2O_2 stimulated Ca^{2+} flux in intracellular *T. gondii* parasites, we investigated the redox state within the parasite cytosol and PV. We reasoned that if calcium release was the direct result of an oxidative signal, the redox status of cellular compartments separating intracellular parasites from the extracellular environment should also be affected. To test this, we generated transgenic parasite strains constitutively expressing the redox sensor protein GRX1-roGFP2, in two different cellular compartments: the parasite cytosol, or targeted to the PV as a consequence of an N-terminal fusion with the GRA8 signal sequence[47]. GRX1-roGFP2 is a ratiometric redox reporter that detects changes in both reduced (GSH) and oxidized (GSSG) glutathione[48] (Figure 3A and B). Importantly, the redox relay system underpinning GRX1-roGFP2 is not affected by pH, which is known to confound data interpretation with other redox sensor proteins[49]. We used GRX1-roGFP2 parasites to track dynamic changes in GSH/GSSG by fluorescence microscopy, and used the normalized GSH/GSSG signal ratio to measure the intensity of oxidation events (Figure 3C – figure supplement 3A). Intracellular parasites expressing the redox sensor targeted to the PV (RH-GRA8-GRX1-roGFP2) or cytosol (RH-GRX1-roGFP2) detected an oxidation event upon exogenous addition of 100 μM H_2O_2 (Figure 3D and E, respectively). The oxidation event within the PV was of greater magnitude compared to that detected within the parasite cytosol, indicating that the strength of the oxidative signal was diminished as it crossed the biological membrane separating these compartments. The water control did not affect the redox signal from GRX1-roGFP2 sensor (Figure 3 – figure supplement 3B).

Having observed that H_2O_2 could stimulate calcium flux, we investigated the reciprocal nature of this relationship by testing the ability of calcium ionophores to trigger an oxidative event. Using GRX1-roGFP2 parasites, we measured the resting redox state prior to ionomycin-induced egress. Ionomycin-induced egress was not accompanied by detectable changes in redox within either the PV or parasite cytosol (Figure 3F and G, respectively). The ionophore A23187 could not be used because of saturating autofluorescence associated with this small molecule in the fluorescence channel used to measure oxidation (Figure 3 – figure supplemental 3C). These data suggested that no significant change in the GSH/GSSG ratio occurs before parasite egress induced by ionomycin.

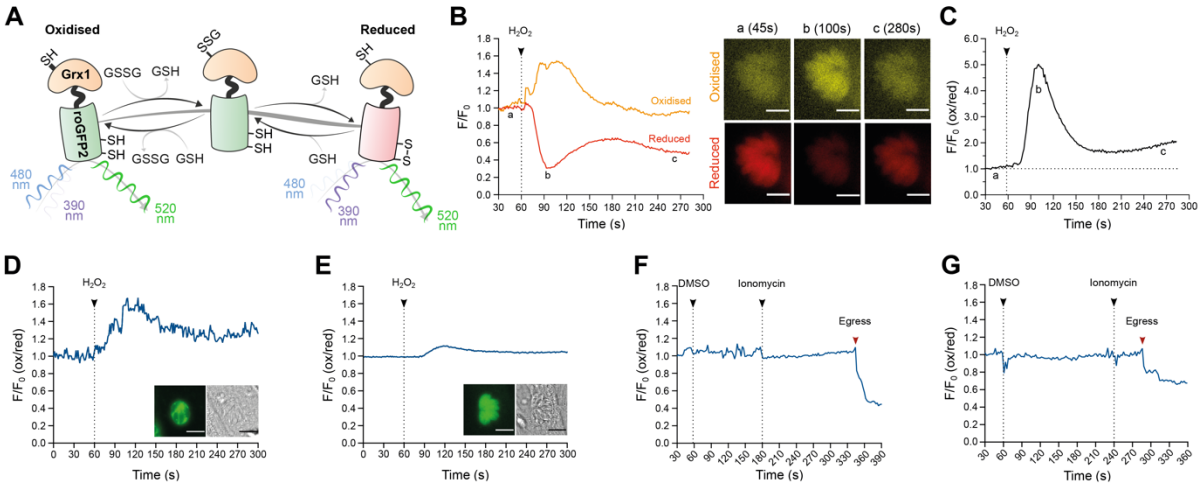

Figure 3: Oxidation induced by exogenous H_2O_2 results in a redox change within the PV and parasite cytosol. (**A**) Schematic representation of the redox sensor based on the catalytic domain of glutaredoxin (GRX1) fused with ro-GFP2 depicting how this sensor interacts with GSH/GSSG and the excitation and emission values of the reduced and oxidized states. (**B** – **C**) Proof-of-principle tracking dynamic changes of GSH/GSSG during an oxidation event in RH-GRX1-roGFP2 parasites. (**B**) Representative signal trace from the GRX1-roGFP2 sensor monitoring both fluorescence channels for reduced (red line) and oxidized (orange line) readouts over time following treatment with 10 mM H_2O_2. Microscopy images of an infected vacuole presented in pseudocolor (orange for oxidation, red for reduction) at a: baseline (45s), b: at the peak of the oxidation event (100s) and c: the return to baseline (280s). This is a representative trace from two independent experiments, with eight vacuoles. Scale bar: 5 µm. (**C**) Presents the oxidation/reduction ratio of normalized signal from graph **B** depicting the intensity changes in redox compared to baseline upon addition of 10 mM H_2O_2. (**D**) Representative trace from RH-GRA8-GRX1-roGFP2 parasites depicting 100 µM H_2O_2 induced redox change within the PV. Microscopy images of an infected vacuole highlighting the presence of the sensor within PV (left image), alongside the brightfield image of the infected host cell. (**E**) A representative trace from RH-GRX1-roGFP2 parasites depicting 100 µM H_2O_2 induction of redox change within the parasite cytosol. Microscopy images depicting an infected vacuole highlighting the presence of the sensor on cytosol (left panel image) alongside the brightfield image of the infected host cell. (**D** – **E**): Representative traces from three independent experiment, nine vacuoles for each group. Scale bar: 5 µm. (**F** and **G**): Representative trace of redox fluctuations in intracellular parasite following 1 µM ionomycin treatment for RH-GRA8-GRX1-roGFP2 (**F**), and RH-GRX1-roGFP2 parasites (**G**). (**E** – **F**): red arrows indicate the moment of parasite egress. Representative traces from three independent experiments, nine vacuoles for each group.

GRX1-roGFP2 redox sensor affects parasite fitness during asexual replication

We noted that one unavoidable result of using the GRX1-roGFP2 redox relay sensors would be the associated overexpression of the catalytic domain of glutaredoxin (as a consequence of it being fused to roGFP2). GRX1 is a small redox enzyme that confers protection against oxidative stress[49, 50], and the overexpression of this enzyme would be expected to shift GSH/GSSG ratios in favour of the reduced form (GSH). Correspondingly, we hypothesized that *T. gondii* strains overexpressing GRX1 would have their normal redox status shifted to a more reduced potential. To test whether the overexpression of this redox protein affected parasite asexual growth, we generated a transgenic parasite strain expressing a version of the redox sensor where we had mutated the key catalytic cysteine residue of GRX to render it enzymatically inactive ($GRX1_{ser}$-roGFP2). As a result, GRX1ser-roGFP2 sensor did not respond changes in GSH/GSSG following H_2O_2 treatment (Figure 4 - figure supplement 4). We compared the growth of this strain with parasites expressing the catalytically active version of the sensor. As before, both active and inactive versions of the GRX-fusion sensor were targeted to either the parasite cytosol or PV. As a control group, we used a parasite strain expressing redox-insensitive sensor GFP (RH-GFP-Luc)[51]. Parasites expressing catalytically active GRX1 in the cytosol presented fewer plaques compared to RH-GFP-Luc (Figure 4A). Despite being able to successfully maintain PV-targeted sensor strains in culture, all parasites lines where the sensor was targeted to the PV did not form clear measurable plaques after six days of growth. Intensely stained plaque-shaped boundaries visible on the HFF monolayer suggested these parasites had successfully grown, but that parasite lytic growth had not outcompeted host cell monolayer recovery sufficiently to produce a clear zone of lysis (Figure 4B). When either the catalytically active or inactive sensors were targeted to the parasite cytosol, parasites formed smaller plaques compared to the RH-GFP-Luc control (Figure 4B and 4C, respectively). These data suggested that the presence roGFP2 alone might be sufficient to affect parasite growth. To directly test the influence of redox environment on the lytic cycle, we grew RH-GFP-Luc parasites with 10 µM N-acetyl cysteine (NAC), a small antioxidant molecule that functions by donating cysteine to increase GSH biosynthesis[52]. Addition of NAC decreased the size of plaques generated by RH-GFP-Luc parasites (Figure 4C), suggesting that GSH/GSSG imbalance compromised parasite growth. To better understand the impact

of overexpressing the sensor on parasite growth, we counted the number of parasites per vacuole after 20 hours of asexual parasite replication (Figure 4D). All strains expressing the redox sensor had reduced replication compared to RH-GFP-Luc (Figure 4 – figure supplement 5), with catalytic inactivation of the GRX domain providing a partial rescue of the replication defect. Strains exhibiting the slowest replication were those where the sensor was targeted to the PV, supporting the plaque growth data in Figure 4B. Together, these data suggest parasite growth is sensitive to changes in GSH/GSSG ratios.

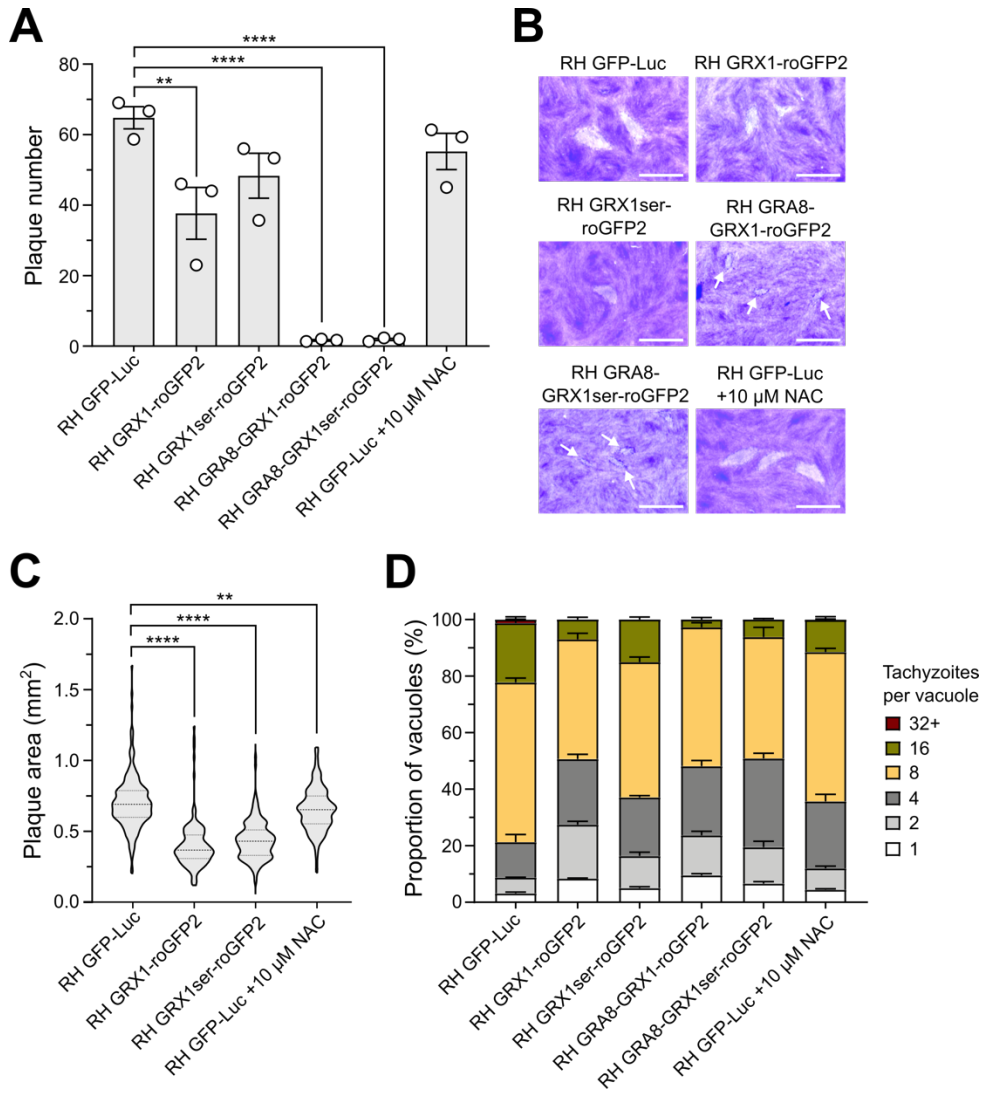

Figure 4: The GRX1-roGFP redox sensor affects *T gondii* asexual replication. (**A**) Histogram presenting plaque count data from a six-day plaque assay using RH-GFP-Luc parasites as a reference control group. (**B**) Representative images of plaques formed. Small plaques are indicated by white arrows. Scale bar: 2 mm. (**C**) Violin plot presenting the distribution of plaque areas (mm^2) for parasites expressing the redox sensor within the cytosol. (**D**) Histogram presenting the effect of the GRX1-roGFP sensors and NAC on parasite intracellular replication. (**A** – **D**) All obtained from three independent experiments, with three technical replicates. Significance was calculated using one-way Anova, Bonferroni's multiple comparisons test for (**A**) and (**B**). P values: **< 0.01, **< 0.001 and ****< 0.0001. The significance analyse for (**D**) is provide on figure supplement 5.

Discussion

Investigations of ROS and *T. gondii* biology initially focused on the host innate immune response. Host macrophages can generate oxidative bursts, creating a toxic microenvironment to fight microbial infection[53-55], with early studies interested in mechanisms used by *T. gondii* to evade oxidative stress[56-58]. However, increasing evidence from multiple organisms has demonstrated that H_2O_2 has functions as a signaling molecule (reviewed in [59]), suggesting the likelihood of a more complex role for ROS in the pathophysiology of *T. gondii*. To sense, respond, and protect against potential oxidative damage from ROS stimuli, cells employ a network of redox-associated proteins such as Trxs, PDIs, Prxs, Grxs, superoxide dismutase and catalase. It was previously shown that *T. gondii* possesses all these elements[26], and we provide an update on the number, diversity and cellular distribution of these redox-associated proteins (Fig. 1). The function of some of these redox-associated gene products in *T. gondii* parasites has been examined: disruption of catalase decreases parasite virulence in mice and *in vitro* tolerance to H_2O_2 [26]; peroxiredoxin-1 interacts with histone lysine methyltransferase to likely regulate gene expression by chromatin rearrangement[60]; two thioredoxins have essential roles in apicoplast biogenesis[61], and another thioredoxin with cytosolic localization has been associated with parasite virulence[62]. Nevertheless, functional information for most of the redox-associated proteins identified in this work remains elusive.

The ability of low concentrations of H_2O_2 to initiate an intracellular Ca^{2+} response in mammalian systems is well documented[63-65] and has helped to solidify H_2O_2 as a signaling molecule. Addition of antioxidants blocks intracellular Ca^{2+} release induced by H_2O_2 in smooth muscle cells[65] suggesting that the oxidative properties of H_2O_2 are required for Ca^{2+} signaling. In human endothelial cells, oxidation induced by non-toxic concentrations of H_2O_2 target a Ca^{2+} channel located in acid compartments[64]. Distinct from these models, this work is the first to report that an oxidation event induced by H_2O_2 mobilizes intracellular Ca^{2+} in *T. gondii* tachyzoites within the infected host cell (Fig. 2A). This is the first time this has been shown for any apicomplexan parasite. Studying the parasite within the host cell provides the best approximation of physiological conditions to observe both Ca^{2+} and redox signaling. Moreover, using parasites expressing a genetically encoded fluorescent Ca^{2+} sensor abrogated the need to use fluorescent Ca^{2+} indicator dyes. Use of these dyes can be damaging

to the cells, and typically require the use of other small molecules to avoid dye loss and compartmentalization[66]. GFP co-expressed with Ca^{2+} sensor allows Ca^{2+} responses to be distinguished from parasite movement which avoids the need to use inhibitors of parasite motility such as cytochalasin D[67]. Finally, the concentration of 100 µM H_2O_2 has been showed to be non-toxic for human fibroblast[68]. Altogether, our protocol to investigate intracellular Ca^{2+} release following H_2O_2 treatment sought to avoid cellular stress that could compromise the true redox/Ca^{2+} dynamic within the parasite. As previously report in muscle cells[65], the presence of antioxidant inhibited the parasite Ca^{2+} response triggered by H_2O_2. Using the GRX1-roGFP2 redox sensor, we confirmed that intracellular parasites directly sense an oxidation event following the exogenous addition of 100 µM H_2O_2. It is not clear whether the exogenous addition of 100 µM of H_2O_2 results in H_2O_2 reaching the intracellular parasites as the host cell contains an extensive network of antioxidant proteins that would be expected to scavenge and neutralise H_2O_2. This could be directly addressed in future experiments using *T. gondii* strains expressing a sensor to specifically detect H_2O_2[69].

Regardless of whether Ca^{2+} is mobilized within the parasite as a direct result of an interaction with H_2O_2, or via secondary oxidation signal from the host, Ca^{2+} regulates all aspects of parasite host cell invasion[9] included egress[16]. For the short time period used to track parasites by microscopy, the intensity of the Ca^{2+} signal spike induced by H_2O_2 was quite modest compared to A23187, and that likely explains why egress events were rare. Longer incubations with H_2O_2 induced parasite egress through a mechanism that requires CDPK3 and likely phosphatidic acid. This is the first evidence that suggests that oxidation can trigger *T. gondii* egress. Interestingly, at the other end of the redox spectrum, the reductive molecule DDT can also mobilize Ca^{2+} and induce parasite egress[31]. Although the mechanism by which H_2O_2 and DDT lead to parasite egress appears to be distinct, these data indicate that redox can influence the parasite's lytic cycle. We anticipate that parasite biology is tuned to a specific environmental redox potential, and that the perturbation of redox homeostasis with either oxidative or reductive stress elicits a phenotypic response.

The mechanism for how H_2O_2 mobilizes Ca^{2+} in animals is better understood but the evolutionary distance between vertebrates and *T. gondii* makes direct comparisons more challenging. *T. gondii* is more closely related to plants, and shares a more similar signaling toolkit[70]. It has been

recently reported that plants possess a cell surface H_2O_2 receptor that once activated, triggers a Ca^{2+} influx into the cells through a Ca^{2+} ion channel[71]. *T. gondii* also has a H_2O_2-sensitive protein that associates with the CDPK1 to promote microneme secretion[33], an event that requires Ca^{2+} mobilization to allow parasite invasion[72].

Our work suggests a connection between oxidation and parasite Ca^{2+} release but our data did not find evidence that ionophore-induced Ca^{2+} release changes the redox state of either the parasite's cytosol or PV. The use of the GRX1-roGFP2 sensor to track redox changes based on GSH/GSSG allows a fast and selective assessment of redox fluctuations in real time [48], with improved dynamics compared to other redox sensors like roGFP1 or roGFP2[73]. Considering that Ca^{2+} mobilization is also a fast event, GRX1-roGFP2 is a suitable tool to investigate the relationship between ROS and Ca^{2+}. Moreover, the fact that GRX1 does not directly interact with H_2O_2 [49] implies this sensor would not interfere with any eventual interaction between H_2O_2 and its potential targets within the parasite or PV. Unexpectedly, expression of GRX1-roGFP2 within *T. gondii* parasites was detrimental to asexual replication. This is surprising as the GRX1-based sensor is generally well tolerated, and presents negligible toxicity in neurons[49, 74]. Inactivation of the catalytic domain of GRX1 only partially recovered parasite growth, suggesting that roGFP2 alone is sufficient to influence parasite replication. Cells contain millimolar concentrations of GSH within their cytoplasm and organelles, and under physiological conditions the cell maintains the majority of this redox buffer molecule in a reduced form ([GSH]>[GSSG])[75]. Parasites overexpressing GRX1 would be expected to affect the normal GSH/GSSG balance. The addition of NAC, a small molecule that can be used to generate GSH, also slowed parasite growth. This supports the hypothesis that the GSH/GSSG ratio can influence parasite replication. Parasites expressing GRX1ser-roGFP2 are likely have altered redox potential due ability of roGFP2 not fused with an active GRX1 to interact directly with oxidizing molecules like H_2O_2[76].

Targeting of the redox sensor to the PV had the greatest effect upon parasite asexual growth. During asexual replication within host cells, *T. gondii* resides within the PV. This compartment separates the parasite from the host cytoplasm, providing a niche for parasite survival and replication[77]. Signaling molecules from the host must cross the PV in order to reach the parasite. Should an oxidative signal from the host encounter an unusually reductive environment within the PV

due the buffering effect of the redox sensor, the signal could be lost before reaching the parasite. Our work increases our understanding of the complex redox system in *T. gondii,* and provides the first evidence that parasite replication is sensitive to redox imbalance. Redox clearly has an important role in *T. gondii* pathophysiology and we anticipate that the unveiling of this network will guide future covalent drug discovery targeting redox-sensitive chemically reactive cysteines.

Material and Methods

Parasite and host cell culture: *T. gondii* tachyzoites from strain RH (Type I) lacking hypoxanthine-guanine phosphoribosyl transferase gene (HXGPRT) were cultivated *in vitro* on monolayers of primary human foreskin fibroblast (HFF, ATTC®) in a humidified incubator at 37°C, 5% CO_2, 3% O_2 atmosphere and maintained in Dulbecco's Modified Eagle medium (DMEM) supplemented with 10% of foetal bovine serum (FBS) and 2mM L-glutamine, without antibiotics. All culture were tested against *Mycoplasma* infection on a monthly basis.

Generation of plasmids and transgenic parasites: All primers used in this study are listed in table supplement 2. The GRX1-roGFP2 sensor[48, 78] was amplified from the commercially available vector pEIGW-GRX1-roGFP2 (Addgene plasmid nº64990) using primers 1/2 and insert into digested (HF-EcoRI & PacI) pTUB8 vector containing selectable marker for HXGPRT using Gibson Assembly® Master Mix. The same strategy was used for GRA8-GRX1-roGFP2, using primers 2/3. To generate vectors with the inactivated GRX1 catalytic domain ($GRX1_{cys23-26}$)[79, 80], primers 4/5 were used to replace cysteine with a serine on pTUB8::GRX1-roGFP2 and primers 4/6 on pTUB8::GRA8-GRX1-roGFP2, followed circularization with KLD reaction mix (NEB), resulting the vectors pTUB8::$GRX1_{(ser23-26)}$-roGFP2 and pTUB8::GRA8-$GRX1_{(ser23-26)}$-roGFP2. All vectors were linearized and transfected into RHΔ*ku80*Δ*HXGPRT* parasites as previously described[81]. Transfected parasites were selected 24 hrs post-transfection by addition of mycophenolic acid (MPA; 25µg/mL) and xanthine (XAN; 50 µg/mL) to culture medium. Strains were cloned by limiting dilution into 96 well plates, and five clones selected. Genomic DNA was extracted from extracellular tachyzoites using

464 Monarch® Genomic DNA Purification Kit (New England BioLabs). Presence of GRX1-based sensors
465 was confirmed using primer pair 7/8.

466 To generate the calcium sensor construct pUPRT::GFP-T2A-jRCaMP1b, sequence encoding
467 the red fluorescent calcium sensor protein jRCaMP1b[41] was ordered from IDT as a custom synthetic
468 gene, and PCR amplified with appropriate Gibson overhangs using primers 9/10. The 5'UTR of
469 *GRA1* was PCR amplified from pTKO2c[82] using primers 11/12, and the GFP-T2A fusion sequence
470 was amplified from an unpublished in-house plasmid using primers 13/14. All three fragments were
471 subsequently cloned by Gibson assembly into PacI-digested UPRT targeting vector pUPRT-HA[83].
472 The resulting construct was linearised using NaeI and transfected into RH Δ*ku80*Δ*hxgprt* parasites to
473 generate the GFP-T2A-jRCaMP1b calcium sensor line. Transgenic parasites were subjected to 5'-
474 fluo-2'-deoxyuridine (FUDR) selection (5 µM) 24 hrs after transfection. To generate the GFP-T2A-
475 jRCaMP1b Δ*CDPK3* line, the *HXGPRT* casette (flanked by 5' and 3' DHFR UTR sequences) was
476 PCR amplified from *pGRA*-HA_HXGPRT[84] using primers 15/16 (introducing 40bp CDPK3
477 homology regions to the amplified fragment) and co-transfected into RH Δ*ku80*Δ*HXGPRT* with
478 pSag1::Cas9-U6::dbl-sgCDPK3. The pSag1::Cas9-U6::dbl-sgCDPK3 vector was generated by
479 inverse PCR amplification of the pSag1::Cas9-U6[85] vector using primer pairs 17/18 and 17/19 to
480 generate intermediate constructs pSag1::Cas9-U6::sg1CDPK3 (comprising sgRNA1) and
481 pSag1::Cas9-U6::sg2CDPK3 (comprising sgRNA2) respectively. Following circularization of both
482 intermediate constructs using KLD reaction mix, a region comprising sgRNA1 was PCR amplified
483 with primers 20/21 from pSag1::Cas9-U6::sg1CDPK3 and Gibson assembled into Kpn1/XhoI
484 linearised pSag1::Cas9-U6:: sg2CDPK3 to generate the double sgRNA plasmid pSag1::Cas9-U6::dbl-
485 sgCDPK3. Recombinant parasites were selected 24 hrs post transfection as previously described for
486 GRX1-roGFP2. Integration of the HXGPRT cassette at the CDPK3 locus was confirmed using primer
487 pairs 22/23 and 24/25 to confirm 5' and 3' integration respectively. Absence of the endogenous
488 CDPK3 locus was confirmed using primers 26/27. RH-GFP-Luc parasites (expressing GFP mutant 3
489 and firefly luciferase IAV[51]) were a gift from Dr Moritz Treeck.
490

Identification of *T. gondii* genes related to redox: Within the *Toxoplasma* database (ToxoDB[35], release 50 beta 17 Dec 2020), a list of genes related to redox signaling in *T. gondii* were obtained using the keywords "thioredoxin", "glutathione", "glutaredoxin", "peroxiredoxin" and "protein disulfide" on gene text search option. The function domains of the canonical antioxidant groups Trxs, Grx-GSH, Prxs and PDIs were confirmed for each gene using Basic Local Alignment Search Tool (BLAST) at National Center for Biotechnology information (NCBI) database (www.ncbi.nlm.nih.gov/). The spatial protein localization related to each redox gene were extracted from the localisation of organelle proteins by isotope tagging (hyperLOPIT)[38, 86] dataset available through ToxoDB.

Plaque and replication assays: For plaque assays, tachyzoites were harvested from infected HFF by syringe passage followed by filtration (5µm). ~100 tachyzoites were added per well of a 6-well plate prepared with confluent HFF monolayers, and allowed to grow undisturbed for 6 days. Plates were washed with phosphate-buffer saline (PBS) and fixed with cold methanol, stained with crystal violet and scanned. Plaque counts and area measurements were performed using FIJI software by drawing region of interesting (ROI). For replication assays, the freshly lysed tachyzoites were added to HFF monolayers grown on a µ-slide 8 well glass bottom chamber (Ibidi®) with multiplicity of infection (MOI) 1. To synchronize the infection, parasites were allowed to settle onto chilled host cells for 20 minutes, and then allowed to invade for 2 hours at 37˚C. Cells were washed with PBS to remove extracellular tachyzoites. Cells were incubated for a further 18 hours, and subsequently fixed with 3% paraformaldehyde at room temperature (RT) for 20 min, and blocked with PBS supplemented with 2% FBS. Parasites per vacuole were counted by excitation with 470nm laser (4% intensity) widefield Nikon Eclipse Ti-E inverted microscope equipped with an ORCA- Flash4.0 camera (Hamamatsu, Japan) and NIS-Elements Viewer software (Nikon), 60x-oil objective. All parasite strains were genetically encoding for GFP or roGFP2. All strains were tested tree independent times, each with three technical replicates.

Egress assay: Freshly lysed tachyzoites from RH-GFP-t2a-jRCaMP1b or RH-GFP-T2A-jRCaMP1bΔ*CDPK3* parasites were harvested and inoculated (MOI:1) onto confluent HFF cells grown on 24 well plates and grown for 18 hours. Cells were washed with PBS and the growth medium replaced with phenol red free DMEM without FBS and incubate for a further three hours. Medium was removed and cells were incubated for 30 minutes with PBS plus drugs (A23187, R59022, H_2O_2) or vehicle controls (water, DMSO). At the end of incubation, the supernatant of the wells was carefully aspirated and cells were detached by 10 min incubation with 200 µL of RT Accutase™. Accutase-release cell suspensions were fixed with 200 µL of 8% paraformaldehyde (20 minutes, RT). Fixed cells were transferred into falcon 5 mL tube with 35 µm nylon mesh cap. Free fluorescent parasite and infected HFF population were analysed and quantified in a BD LRSFortessa™. A total of 5000 events were collected for each tube. Blue laser (488nm) with 530/30 nm filter was used to detect the GFP signal. An uninfected HFF control was used to assess the effect of each drug treatment on host cell gating. Each drug condition was tested two independent times, each with six technical replicates.

Fluorescence microscopy: For cytosolic Ca^{2+} fluorometric measurements, RH-GFP-T2A-jRCaMP1b or RH-GFP-T2A-jRCaMP1bΔ*CDPK3* parasites were added (MOI:1) to confluent HFF grown on 8 well glass bottom chamber and allowed to grow for 18 hours. Wells were washed with PBS and media replaced by phenol red-free DMEM medium without FBS, and incubate for a further two hours. Images of live infected HFFs were captured at 37°C, using a 60x-oil objective in the same widefield microscope previously describe on replication assay. GFP (470 nm excitation/ 520 nm emission) and jRCaMP1b (555 nm excitation/ 605 nm emission) with 100 milliseconds acquisition rate signal were collected every second for up to a maximum 10 minutes. Drugs were applied on the wells after one minute of acquisition by pipetting. Image analyses were performed using FIJI software. Raw fluorescence readout (F) for each vacuole on each channel was normalised against the average of the baseline signal before adding the drug (F_0) using the ratio F/F_0 bringing the resting baseline value to one. To distinguish intracellular Ca^{2+} oscillation signal from vacuole movement, the

545 $F_{(jRCaMP1b)}/F_{0(jRCaMP1b)}$ values were normalised against the GFP signal $F_{(GFP)}/F_{0(GFP)}$. Ca^{2+} response
546 during a specific time is given by the formula: $(F_{(jRCaMP1b)}/F_{0(jRCaMP1b)}) / (F_{(GFP)}/F_{0(GFP)})$.
547 For redox measurements, parasites expressing ratiometric GRX1 based sensors were treated as
548 described for RH-GFP-T2A-jRCaMP1b parasites. Oxidized GRX1-roGFP2 (395 nm excitation/ 520
549 nm emission) and reduced GRX1-roGFP2 (470 nm excitation/ 520 nm emission) with 200
550 milliseconds acquisition rate signal were collected every second for up to a maximum 10 minutes.
551 Data analyses is similar to Ca^{2+}, the redox reading was obtained by formula: $(F_{(oxidised)}/F_{0(oxidised)}) /$
552 $(F_{(reduced)}/F_{0(reduced)})$.
553
554 **Chemical and Reagents:** Hydrogen peroxide 30% (w/w) solution with stabilizer; diacylglycerol
555 kinase inhibitor (R59022); A23187, Ionomycin, anhydrous methanol, and crystal violet solution were
556 obtained from Sigma-Aldrich Company Ltd. α-tocopherol phosphate disodium salt from Merk.
557 Dimethylsulfoxide (DMSO) anhydrous and paraformaldehyde 16% solution from Life Technologies.
558 Accutase cell detachment solution from Fisher Scientific Ltd.
559
560 **Statistical Analysis:** The data are represented as the mean ± SEM and analysed using two-
561 tailed pared Student *t* test between two groups and one-way or 2way analyses of variance
562 (ANOVA) with Bonferroni's multiple comparisons test for comparing means between ≥3.
563 All data were analysed using GraphPad Prism 9 software (California, USA). The data were
564 considered statistically significant when P values <0.05.
565
566 **Funding**
567 This work was supported by grant 202553/Z/16/Z from the Wellcome Trust & Royal Society (to
568 MAC), and BB/M011178/1 from the BBSRC (to HJB and MAC).
569
570
571

Acknowledgements

We sincerely thank Prof Jake Baum and Dr George Ashdown for the access and assistance to widefield microscopy, Dr Moritz Treeck for the RH-GFP-Luc line, Dr Lilach Sheiner for the roGFP construct, and Dr Gautam Dey for useful discussions. We would also like to thank the Imperial College Flow Cytometry Facility team in South Kensington for technical support. We would like to acknowledge the artistic contribution of Mai Ito who kindly provided the graphical depiction of a *T. gondii* tachyzoite used in Figure 1.

Competing interests

The authors have declared there are no conflict or competing interest.

References

1. Halonen SK, Weiss LM. Toxoplasmosis. Handb Clin Neurol. 2013;114:125-45.

2. Flegr J, Prandota J, Sovickova M, Israili ZH. Toxoplasmosis--a global threat. Correlation of latent toxoplasmosis with specific disease burden in a set of 88 countries. PLoS One. 2014;9(3):e90203.

3. Sheffield HG, Melton ML. The fine structure and reproduction of Toxoplasma gondii. J Parasitol. 1968;54(2):209-26.

4. Dubey JP. WAAP and Pfizer Award for excellence in veterinary parasitology research. Pursuing life cycles and transmission of cyst-forming coccidia of animals and humans. Vet Parasitol. 1996;64(1-2):13-20.

5. Weiss LM, Dubey JP. Toxoplasmosis: A history of clinical observations. Int J Parasitol. 2009;39(8):895-901.

6. Luft BJ, Remington JS. Toxoplasmic encephalitis in AIDS. Clin Infect Dis. 1992;15(2):211-22.

7. Goldman M, Carver RK, Sulzer AJ. Reproduction of Toxoplasma gondii by internal budding. J Parasitol. 1958;44(2):161-71.

8. Montoya JG, Liesenfeld O. Toxoplasmosis. Lancet. 2004;363(9425):1965-76.

600 9. Lourido S, Moreno SN. The calcium signaling toolkit of the Apicomplexan parasites
601 Toxoplasma gondii and Plasmodium spp. Cell calcium. 2015;57(3):186-93.
602 10. Vieira MC, Moreno SN. Mobilization of intracellular calcium upon attachment of
603 Toxoplasma gondii tachyzoites to human fibroblasts is required for invasion. Mol Biochem Parasitol.
604 2000;106(1):157-62.
605 11. Pace DA, McKnight CA, Liu J, Jimenez V, Moreno SN. Calcium entry in Toxoplasma gondii
606 and its enhancing effect of invasion-linked traits. J Biol Chem. 2014;289(28):19637-47.
607 12. Wetzel DM, Chen LA, Ruiz FA, Moreno SN, Sibley LD. Calcium-mediated protein secretion
608 potentiates motility in Toxoplasma gondii. J Cell Sci. 2004;117(Pt 24):5739-48.
609 13. Endo T, Sethi KK, Piekarski G. Toxoplasma gondii: calcium ionophore A23187-mediated
610 exit of trophozoites from infected murine macrophages. Exp Parasitol. 1982;53(2):179-88.
611 14. Murphy RC, Ojo KK, Larson ET, Castellanos-Gonzalez A, Perera BG, Keyloun KR, et al.
612 Discovery of Potent and Selective Inhibitors of Calcium-Dependent Protein Kinase 1 (CDPK1) from
613 C. parvum and T. gondii. ACS Med Chem Lett. 2010;1(7):331-5.
614 15. Ojo KK, Larson ET, Keyloun KR, Castaneda LJ, Derocher AE, Inampudi KK, et al.
615 Toxoplasma gondii calcium-dependent protein kinase 1 is a target for selective kinase inhibitors.
616 Nature structural & molecular biology. 2010;17(5):602-7.
617 16. Garrison E, Treeck M, Ehret E, Butz H, Garbuz T, Oswald BP, et al. A forward genetic
618 screen reveals that calcium-dependent protein kinase 3 regulates egress in Toxoplasma. PLoS Pathog.
619 2012;8(11):e1003049.
620 17. Bullen HE, Jia Y, Yamaryo-Botte Y, Bisio H, Zhang O, Jemelin NK, et al. Phosphatidic
621 Acid-Mediated Signaling Regulates Microneme Secretion in Toxoplasma. Cell Host Microbe.
622 2016;19(3):349-60.
623 18. Brown KM, Lourido S, Sibley LD. Serum Albumin Stimulates Protein Kinase G-dependent
624 Microneme Secretion in Toxoplasma gondii. J Biol Chem. 2016;291(18):9554-65.
625 19. Guzik TJ, West NE, Black E, McDonald D, Ratnatunga C, Pillai R, et al. Vascular superoxide
626 production by NAD(P)H oxidase: association with endothelial dysfunction and clinical risk factors.
627 Circ Res. 2000;86(9):E85-90.

628 20. Winterbourn CC, Hampton MB. Thiol chemistry and specificity in redox signaling. Free
629 Radic Biol Med. 2008;45(5):549-61.
630 21. Pastore A, Piemonte F. S-Glutathionylation signaling in cell biology: progress and prospects.
631 Eur J Pharm Sci. 2012;46(5):279-92.
632 22. Popov D. Protein S-glutathionylation: from current basics to targeted modifications. Arch
633 Physiol Biochem. 2014;120(4):123-30.
634 23. Sabens Liedhegner EA, Gao XH, Mieyal JJ. Mechanisms of altered redox regulation in
635 neurodegenerative diseases--focus on S--glutathionylation. Antioxid Redox Signal. 2012;16(6):543-
636 66.
637 24. Xiong Y, Uys JD, Tew KD, Townsend DM. S-glutathionylation: from molecular mechanisms
638 to health outcomes. Antioxid Redox Signal. 2011;15(1):233-70.
639 25. Murray HW, Cohn ZA. Macrophage oxygen-dependent antimicrobial activity. I.
640 Susceptibility of Toxoplasma gondii to oxygen intermediates. J Exp Med. 1979;150(4):938-49.
641 26. Ding M, Kwok LY, Schluter D, Clayton C, Soldati D. The antioxidant systems in
642 Toxoplasma gondii and the role of cytosolic catalase in defence against oxidative injury. Mol
643 Microbiol. 2004;51(1):47-61.
644 27. Luder CG, Gross U. Apoptosis and its modulation during infection with Toxoplasma gondii:
645 molecular mechanisms and role in pathogenesis. Curr Top Microbiol Immunol. 2005;289:219-37.
646 28. Luder CG, Stanway RR, Chaussepied M, Langsley G, Heussler VT. Intracellular survival of
647 apicomplexan parasites and host cell modification. Int J Parasitol. 2009;39(2):163-73.
648 29. Akerman SE, Muller S. Peroxiredoxin-linked detoxification of hydroperoxides in
649 Toxoplasma gondii. J Biol Chem. 2005;280(1):564-70.
650 30. Kaasch AJ, Joiner KA. Targeting and subcellular localization of Toxoplasma gondii catalase.
651 Identification of peroxisomes in an apicomplexan parasite. J Biol Chem. 2000;275(2):1112-8.
652 31. Stommel EW, Ely KH, Schwartzman JD, Kasper LH. Toxoplasma gondii: dithiol-induced
653 Ca2+ flux causes egress of parasites from the parasitophorous vacuole. Exp Parasitol. 1997;87(2):88-
654 97.

655 32. Silverman JA, Qi H, Riehl A, Beckers C, Nakaar V, Joiner KA. Induced activation of the
656 Toxoplasma gondii nucleoside triphosphate hydrolase leads to depletion of host cell ATP levels and
657 rapid exit of intracellular parasites from infected cells. J Biol Chem. 1998;273(20):12352-9.
658 33. Child MA, Garland M, Foe I, Madzelan P, Treeck M, van der Linden WA, et al. Toxoplasma
659 DJ-1 Regulates Organelle Secretion by a Direct Interaction with Calcium-Dependent Protein Kinase 1.
660 mBio. 2017;8(1).
661 34. Augusto L, Martynowicz J, Amin PH, Carlson KR, Wek RC, Sullivan WJ. TgIF2K-B is an
662 eIF2α kinase in Toxoplasma gondii that responds to oxidative stress and optimizes
663 pathogenicity. bioRxiv. 2020:2020.09.24.312744.
664 35. Gajria B, Bahl A, Brestelli J, Dommer J, Fischer S, Gao X, et al. ToxoDB: an integrated
665 Toxoplasma gondii database resource. Nucleic Acids Res. 2008;36(Database issue):D553-6.
666 36. Odberg-Ferragut C, Renault JP, Viscogliosi E, Toursel C, Briche I, Engels A, et al. Molecular
667 cloning, expression analysis and iron metal cofactor characterisation of a superoxide dismutase from
668 Toxoplasma gondii. Mol Biochem Parasitol. 2000;106(1):121-9.
669 37. Sibley LD, Lawson R, Weidner E. Superoxide dismutase and catalase in Toxoplasma gondii.
670 Mol Biochem Parasitol. 1986;19(1):83-7.
671 38. Barylyuk K, Koreny L, Ke H, Butterworth S, Crook OM, Lassadi I, et al. A Comprehensive
672 Subcellular Atlas of the Toxoplasma Proteome via hyperLOPIT Provides Spatial Context for Protein
673 Functions. Cell Host Microbe. 2020;28(5):752-66 e9.
674 39. Meissner G. Regulation of mammalian ryanodine receptors. Front Biosci. 2002;7:d2072-80.
675 40. Oda T, Yang Y, Uchinoumi H, Thomas DD, Chen-Izu Y, Kato T, et al. Oxidation of
676 ryanodine receptor (RyR) and calmodulin enhance Ca release and pathologically alter, RyR structure
677 and calmodulin affinity. J Mol Cell Cardiol. 2015;85:240-8.
678 41. Dana H, Mohar B, Sun Y, Narayan S, Gordus A, Hasseman JP, et al. Sensitive red protein
679 calcium indicators for imaging neural activity. Elife. 2016;5.
680 42. Black MW, Arrizabalaga G, Boothroyd JC. Ionophore-resistant mutants of Toxoplasma
681 gondii reveal host cell permeabilization as an early event in egress. Mol Cell Biol. 2000;20(24):9399-
682 408.

683 43. Treeck M, Sanders JL, Gaji RY, LaFavers KA, Child MA, Arrizabalaga G, et al. The
684 Calcium-Dependent Protein Kinase 3 of Toxoplasma Influences Basal Calcium Levels and Functions
685 beyond Egress as Revealed by Quantitative Phosphoproteome Analysis. PLoS Pathog.
686 2014;10(6):e1004197.
687 44. Stewart RJ, Whitehead L, Nijagal B, Sleebs BE, Lessene G, McConville MJ, et al. Analysis
688 of Ca(2)(+) mediated signaling regulating Toxoplasma infectivity reveals complex relationships
689 between key molecules. Cell Microbiol. 2017;19(4).
690 45. Cooke E, Al-Mohanna FA, Hallett MB. Diacylglycerol kinase inhibitor, R59022, potentiates
691 neutrophil oxidase activation by Ca2+-dependent stimuli. Evidence for two separate but convergent
692 pathways. Biochem Pharmacol. 1987;36(20):3459-62.
693 46. Bullen HE, Bisio H, Soldati-Favre D. The triumvirate of signaling molecules controlling
694 Toxoplasma microneme exocytosis: Cyclic GMP, calcium, and phosphatidic acid. PLoS Pathog.
695 2019;15(5):e1007670.
696 47. Carey KL, Donahue CG, Ward GE. Identification and molecular characterization of GRA8, a
697 novel, proline-rich, dense granule protein of Toxoplasma gondii. Mol Biochem Parasitol.
698 2000;105(1):25-37.
699 48. Aller I, Rouhier N, Meyer AJ. Development of roGFP2-derived redox probes for
700 measurement of the glutathione redox potential in the cytosol of severely glutathione-deficient rml1
701 seedlings. Front Plant Sci. 2013;4:506.
702 49. Gutscher M, Pauleau AL, Marty L, Brach T, Wabnitz GH, Samstag Y, et al. Real-time
703 imaging of the intracellular glutathione redox potential. Nat Methods. 2008;5(6):553-9.
704 50. Laporte D, Olate E, Salinas P, Salazar M, Jordana X, Holuigue L. Glutaredoxin GRXS13
705 plays a key role in protection against photooxidative stress in Arabidopsis. J Exp Bot.
706 2012;63(1):503-15.
707 51. Ploemen IH, Prudencio M, Douradinha BG, Ramesar J, Fonager J, van Gemert GJ, et al.
708 Visualisation and quantitative analysis of the rodent malaria liver stage by real time imaging. PLoS
709 One. 2009;4(11):e7881.

710 52. Ezerina D, Takano Y, Hanaoka K, Urano Y, Dick TP. N-Acetyl Cysteine Functions as a Fast-
711 Acting Antioxidant by Triggering Intracellular H2S and Sulfane Sulfur Production. Cell Chem Biol.
712 2018;25(4):447-59 e4.
713 53. Dupre-Crochet S, Erard M, Nubetae O. ROS production in phagocytes: why, when, and
714 where? J Leukoc Biol. 2013;94(4):657-70.
715 54. McLeod R, Estes R, Mack DG, McLeod EG. Effects of human alveolar macrophages and
716 peripheral blood monocytes on Toxoplasma gondii. J Infect Dis. 1983;147(5):957.
717 55. Sibley LD, Krahenbuhl JL, Weidner E. Lymphokine activation of J774G8 cells and mouse
718 peritoneal macrophages challenged with Toxoplasma gondii. Infect Immun. 1985;49(3):760-4.
719 56. Wilson CB, Tsai V, Remington JS. Failure to trigger the oxidative metabolic burst by normal
720 macrophages: possible mechanism for survival of intracellular pathogens. J Exp Med.
721 1980;151(2):328-46.
722 57. Shrestha SP, Tomita T, Weiss LM, Orlofsky A. Proliferation of Toxoplasma gondii in
723 inflammatory macrophages in vivo is associated with diminished oxygen radical production in the
724 host cell. Int J Parasitol. 2006;36(4):433-41.
725 58. Lima TS, Lodoen MB. Mechanisms of Human Innate Immune Evasion by Toxoplasma
726 gondii. Front Cell Infect Microbiol. 2019;9:103.
727 59. Veal E, Day A. Hydrogen peroxide as a signaling molecule. Antioxid Redox Signal.
728 2011;15(1):147-51.
729 60. Sautel CF, Ortet P, Saksouk N, Kieffer S, Garin J, Bastien O, et al. The histone methylase
730 KMTox interacts with the redox-sensor peroxiredoxin-1 and targets genes involved in Toxoplasma
731 gondii antioxidant defences. Mol Microbiol. 2009;71(1):212-26.
732 61. Biddau M, Bouchut A, Major J, Saveria T, Tottey J, Oka O, et al. Two essential Thioredoxins
733 mediate apicoplast biogenesis, protein import, and gene expression in Toxoplasma gondii. PLoS
734 Pathog. 2018;14(2):e1006836.
735 62. Xue J, Jiang W, Chen Y, Gong F, Wang M, Zeng P, et al. Thioredoxin reductase from
736 Toxoplasma gondii: an essential virulence effector with antioxidant function. FASEB J.
737 2017;31(10):4447-57.

738 63. Volk T, Hensel M, Kox WJ. Transient Ca2+ changes in endothelial cells induced by low
739 doses of reactive oxygen species: role of hydrogen peroxide. Mol Cell Biochem. 1997;171(1-2):11-21.
740 64. Avdonin PV, Nadeev AD, Tsitrin EB, Tsitrina AA, Avdonin PP, Mironova GY, et al.
741 Involvement of two-pore channels in hydrogen peroxide-induced increase in the level of calcium ions
742 in the cytoplasm of human umbilical vein endothelial cells. Dokl Biochem Biophys. 2017;474(1):209-
743 12.
744 65. Roveri A, Coassin M, Maiorino M, Zamburlini A, van Amsterdam FT, Ratti E, et al. Effect of
745 hydrogen peroxide on calcium homeostasis in smooth muscle cells. Arch Biochem Biophys.
746 1992;297(2):265-70.
747 66. Di Virgilio F, Steinberg TH, Silverstein SC. Inhibition of Fura-2 sequestration and secretion
748 with organic anion transport blockers. Cell Calcium. 1990;11(2-3):57-62.
749 67. Carter SB. Effects of cytochalasins on mammalian cells. Nature. 1967;213(5073):261-4.
750 68. Hyslop PA, Hinshaw DB, Scraufstatter IU, Cochrane CG, Kunz S, Vosbeck K. Hydrogen
751 peroxide as a potent bacteriostatic antibiotic: implications for host defense. Free Radic Biol Med.
752 1995;19(1):31-7.
753 69. Gutscher M, Sobotta MC, Wabnitz GH, Ballikaya S, Meyer AJ, Samstag Y, et al. Proximity-
754 based protein thiol oxidation by H2O2-scavenging peroxidases. J Biol Chem. 2009;284(46):31532-40.
755 70. Nagamune K, Sibley LD. Comparative genomic and phylogenetic analyses of calcium
756 ATPases and calcium-regulated proteins in the apicomplexa. Mol Biol Evol. 2006;23(8):1613-27.
757 71. Wu F, Chi Y, Jiang Z, Xu Y, Xie L, Huang F, et al. Hydrogen peroxide sensor HPCA1 is an
758 LRR receptor kinase in Arabidopsis. Nature. 2020;578(7796):577-81.
759 72. Lovett JL, Marchesini N, Moreno SN, Sibley LD. Toxoplasma gondii microneme secretion
760 involves intracellular Ca(2+) release from inositol 1,4,5-triphosphate (IP(3))/ryanodine-sensitive
761 stores. J Biol Chem. 2002;277(29):25870-6.
762 73. Hanson GT, Aggeler R, Oglesbee D, Cannon M, Capaldi RA, Tsien RY, et al. Investigating
763 mitochondrial redox potential with redox-sensitive green fluorescent protein indicators. J Biol Chem.
764 2004;279(13):13044-53.

765 74. Hasel P, McKay S, Qiu J, Hardingham GE. Selective dendritic susceptibility to bioenergetic,
766 excitotoxic and redox perturbations in cortical neurons. Biochim Biophys Acta. 2015;1853(9):2066-
767 76.
768 75. Brieger K, Schiavone S, Miller FJ, Jr., Krause KH. Reactive oxygen species: from health to
769 disease. Swiss Med Wkly. 2012;142:w13659.
770 76. Liu X, Wu J, Liu H, Zong N, Zhao J. RoGFP1 is a quantitative biosensor in maize cells for
771 cellular redox changes caused by environmental and endogenous stimuli. Biochem Biophys Res
772 Commun. 2014;452(3):503-8.
773 77. Clough B, Frickel EM. The Toxoplasma Parasitophorous Vacuole: An Evolving Host-
774 Parasite Frontier. Trends Parasitol. 2017;33(6):473-88.
775 78. Meyer AJ, Brach T, Marty L, Kreye S, Rouhier N, Jacquot JP, et al. Redox-sensitive GFP in
776 Arabidopsis thaliana is a quantitative biosensor for the redox potential of the cellular glutathione
777 redox buffer. Plant J. 2007;52(5):973-86.
778 79. Sun C, Berardi MJ, Bushweller JH. The NMR solution structure of human glutaredoxin in the
779 fully reduced form. J Mol Biol. 1998;280(4):687-701.
780 80. Yang Y, Jao S, Nanduri S, Starke DW, Mieyal JJ, Qin J. Reactivity of the human
781 thioltransferase (glutaredoxin) C7S, C25S, C78S, C82S mutant and NMR solution structure of its
782 glutathionyl mixed disulfide intermediate reflect catalytic specificity. Biochemistry.
783 1998;37(49):17145-56.
784 81. Soldati D, Boothroyd JC. Transient transfection and expression in the obligate intracellular
785 parasite Toxoplasma gondii. Science. 1993;260(5106):349-52.
786 82. Caffaro CE, Koshy AA, Liu L, Zeiner GM, Hirschberg CB, Boothroyd JC. A nucleotide
787 sugar transporter involved in glycosylation of the Toxoplasma tissue cyst wall is required for efficient
788 persistence of bradyzoites. PLoS Pathog. 2013;9(5):e1003331.
789 83. Reese ML, Zeiner GM, Saeij JP, Boothroyd JC, Boyle JP. Polymorphic family of injected
790 pseudokinases is paramount in Toxoplasma virulence. Proc Natl Acad Sci U S A. 2011;108(23):9625-
791 30.

792 84. Coppens I, Dunn JD, Romano JD, Pypaert M, Zhang H, Boothroyd JC, et al. Toxoplasma
793 gondii sequesters lysosomes from mammalian hosts in the vacuolar space. Cell. 2006;125(2):261-74.
794 85. Behnke MS, Zhang TP, Dubey JP, Sibley LD. Toxoplasma gondii merozoite gene expression
795 analysis with comparison to the life cycle discloses a unique expression state during enteric
796 development. BMC Genomics. 2014;15:350.
797 86. Crook OM, Mulvey CM, Kirk PDW, Lilley KS, Gatto L. A Bayesian mixture modelling
798 approach for spatial proteomics. PLoS Comput Biol. 2018;14(11):e1006516.
799
800
801
802
803
804
805
806
807
808
809
810
811
812
813
814
815
816
817
818

819 **Supplemental Material**

Gene ID (ToxoDB)	Gene annotation	Predicted localisation	Publication indicating redox function
TGME49_204480	thioredoxin domain-containing protein	apicoplast	no
TGME49_209950	thioredoxin domain-containing protein	apicoplast	no
TGME49_216510	thioredoxin, putative	mitochondria-membrane	no
TGME49_218530	PITH domain-containing protein	cytosol	no
TGME49_240500	PITH domain-containing protein	19S proteasome	no
TGME49_224060	thioredoxin, putative	golgi	no
TGME49_247350	thioredoxin domain-containing protein	ER	no
TGME49_269950	thioredoxin domain-containing protein	dense granules	no
TGME49_201800	thioredoxin domain-containing protein	mitochondria-membrane	no
TGME49_247660	thioredoxin domain-containing protein	NA	no
TGME49_255480	thioredoxin domain-containing protein	NA	no
TGME49_266620	thioredoxin domain-containing protein	ER	yes[1]
TGME49_310770	hypothetical protein / ATrx2	apicoplast	yes[2]
TGME49_265510	hypothetical protein	19S proteasome	no
TGME49_270120	thioredoxin-like protein, TLP1	mitochondria-soluble	no
TGME49_289180	thioredoxin domain-containing protein	mitochondria-soluble	no
TGME49_290260	PITH domain-containing protein	cytosol	yes[1]
TGME49_291810	thioredoxin domain-containing protein	NA	no
TGME49_293870	thioredoxin	cytosol	no
TGME49_271760	seryl-tRNA synthetase (SeRS2)	ER	no
TGME49_270140	splicing factor DIM1, putative	cytosol	no
TGME49_308050	phosducin domain-containing protein	NA	no
TGME49_309730	thioredoxin reductase	cytosol	yes [3]
TGME49_247025	PITH domain-containing protein	NA	no
TGME49_258826	thioredoxin domain-containing protein	ER	no
TGME49_312110	thioredoxin domain-containing protein	apicoplast	yes[4]
TGME49_225060	thioredoxin domain-containing protein	nucleus-chromatin	no
TGME49_211680	protein disulfide-isomerase	ER	yes[5]
TGME49_218470	protein disulfide-isomerase, putative	NA	no
TGME49_225790	thioredoxin-like-fold domain-containing protein	cytoskeleton	no
TGME49_232410	thioredoxin-like-fold domain-containing protein	cytoskeleton	no
TGME49_238040	protein disulfide-isomerase domain-containing protein	ER	no
TGME49_249270	protein disulfide isomerase-related protein (provisional), putative	apicoplast	no
TGME49_226800	GSH-synthase domain-containing protein	nucleolus	
TGME49_238070	glutaredoxin domain-containing protein	cytosol	no
TGME49_277790	glutaredoxin domain-containing protein	PM-peripheral	no
TGME49_304660	glutaredoxin domain-containing protein	mitochondria-soluble	no
TGME49_247580	glutaredoxin domain-containing protein	rhoptries	no
TGME49_227150	glutaredoxin domain-containing protein	apicoplast	no
TGME49_279400	glutaredoxin domain-containing protein	cytosol	no
TGME49_268730	glutaredoxin domain-containing protein	mitochondria-soluble	no
TGME49_246920	glutathione reductase	19S proteosome	no
TGME49_306030	glutathione s-transferase, n-terminal domain containing	ER	no
TGME49_249630	glutathione s-transferase, N-terminal domain-containing protein	mitochondria-soluble	no
TGME49_281630	lactamase-b domain-containing protein	nucleolus	no
TGME49_219130	NADPH-glutathione reductase	apicoplast	no
TGME49_227100	glutaredoxin domain-containing protein	NA	no
TGME49_285920	hypothetical protein	NA	no
TGME49_309210	thioredoxin domain-containing protein / peroxiredoxin 6, putative	cytosol	no
TGME49_230410	thioredoxin domain-containing protein / peroxiredoxin PRX3	mitochondria-soluble	yes[6, 7]
TGME49_266130	glutathione peroxidase / peroxiredoxin PRX2	NA	yes[7]
TGME49_217890	peroxiredoxin / alkyl hydroperoxide reductase	nucleus	yes[8]
TGME49_286630	peroxiredoxin / redoxin domain-containing protein	apicoplast	yes[8]
TGME49_266120	glutathione peroxidase / thioredoxin-dependent peroxidase TPX1	PM-peripheral	yes[9]
TGME49_316330	superoxide dismutase SOD2	mitochondria-soluble	yes[7]
TGME49_232250	catalase	cytosol	yes[7, 10, 11]
TGME49_316190	superoxide dismutase SOD3	NA	yes[7]
TGME49_316310	superoxide dismutase	cytosol	yes[12]

820

Table supplement 1: List of *Toxoplasma gondii* genes related to redox sensing systems and their primary location based on hyperLOPIT datasets. Abbreviations: PITH: proteasome-interacting thioredoxin. ER: endoplasmic reticulum. PM: plasma membrane. GSH: glutathione. NA: not applicable (location not predicted).

Supplemental video 1: Intracellular *T. gondii* tachyzoites mobilize Ca^{2+} upon addition of H_2O_2, followed by egress induced by A23187. The left panel displays the GFP channel, middle panel the Ca^{2+} sensor jCaMP1b channel, and the right panel the channel merge. Time (minutes: seconds) is displayed on the left top region of each channel. 100 µM of H_2O_2 was added to cells at 1:06, and 1 µM A23187 was added at 6:51. Video frame rate: 17 frames per second. This video is representative of 27 infected vacuoles from four independent experiments. MOI: 1.

Supplemental video 2: Hydrogen peroxide inducing egress of *T. gondii* tachyzoites at low MOI. The left panel displays the GFP channel, the middle panel the Ca^{2+} sensor jCaMP1b channel, and the right panel the merge. Time (minutes: seconds) is displayed on the left top region of each channel. 100 µM of H_2O_2 was added to cells at 00:45s. Video frame rate: 10 frames per second. This video presents an egress event captured using low MOI (MOI=1).

Supplemental video 3: Hydrogen peroxide inducing egress of *T. gondii* tachyzoites at high MOI. The left panel displays the GFP channel, middle panel the Ca^{2+} sensor jCaMP1b channel, and the right panel the merge. Time (minutes: seconds) is displayed on the left top region of each channel. 100 µM of H_2O_2 was added to cells at 00:30s. Video frame rate: 15 frames per second. This video is representative of 34 infected vacuoles from three independent experiments (MOI=5).

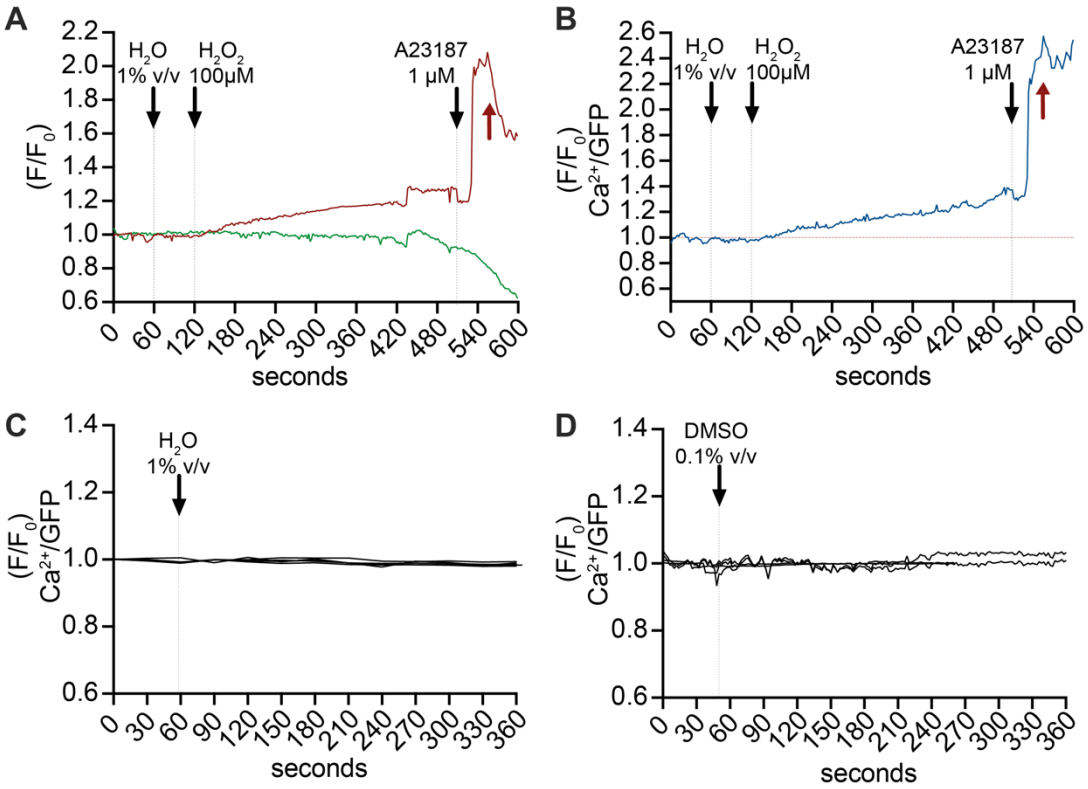

Figure supplement 1: Fluorescence tracking of Ca^{2+} signal and GFP movement on RH-GFP-t2a-jRCaMP1b parasites within host cell. (**A – B**) Representative trace of parasite vacuoles following treatment with H_2O_2 and ionophore A23187. (**A**) The graph presents the independent GFP trace (green) and Ca^{2+} signal from jRCaMP1b sensor (red). Note the parasite movement at 420s. (**B**) Graph of the Ca^{2+} signal is normalized to GFP to minimize artefact on the Ca^{2+} measurements due to parasite movement. Red arrow indicates the moment of parasite egress. (**C**) Water, the vehicle solvent for H_2O_2, does not mobilize Ca^{2+}. The graph displays the trace of three independent vacuoles from the same field of view. Data are representative of 15 infected vacuoles from four independent experiments. (**D**) DMSO, the vehicle solvent for ionophore A23187, does not mobilize Ca^{2+}. The graph displays the trace of four independent infected vacuoles from the same field of view. Data are representative of 12 rosettes from three independent experiments. (**A – D**): black arrows indicate the time of drug / solvent addition.

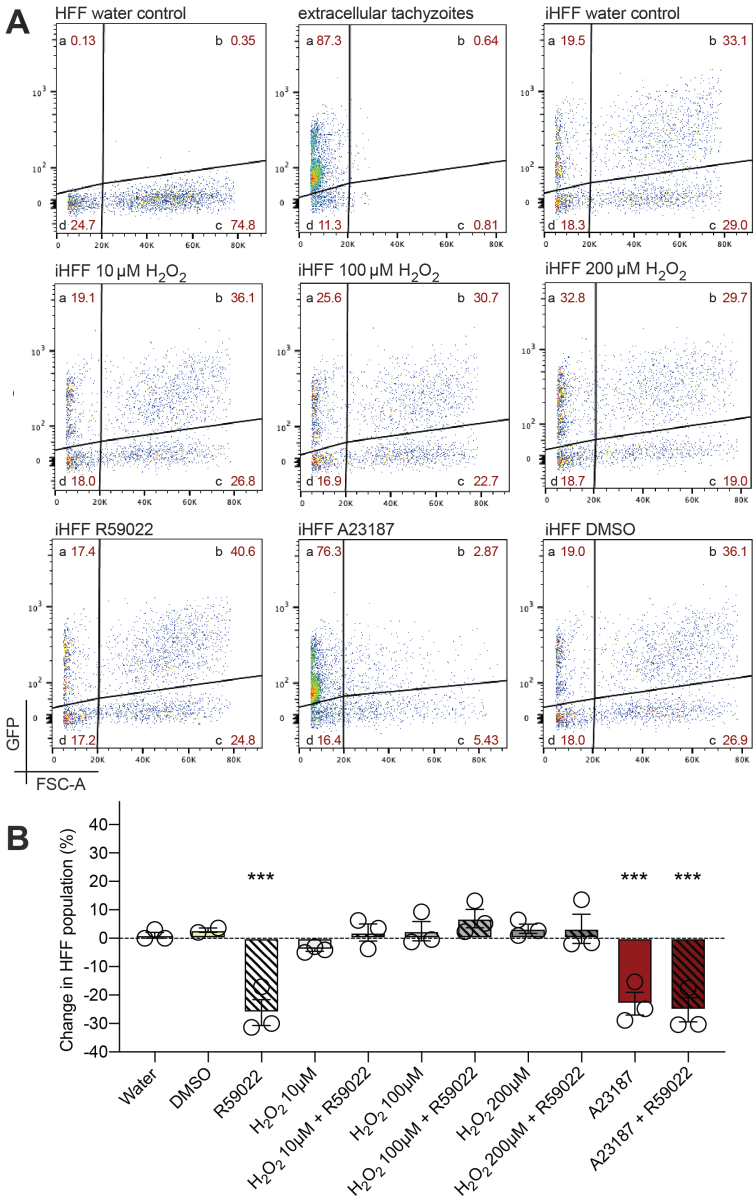

Figure supplement 2: Quantification of RH-GFP-T2A-jCamP1b parasite egress by flow cytometry. (**A**) Representative gating using GFP (Blue laser, 488nm, filter 530/30) against Forward scatter (FSC-A). HFF water control: uninfected human foreskin fibroblast (HFF) are mainly localised in quadrant c. Lysed tachyzoites: free RH-GFP-T2A-jCamP1b parasites are mainly localised in quadrant a. iHFF water control: infected host cells are detected in quadrant b. By using the GFP it is possible to distinguish free fluorescent parasite from iHFF in a population and assess the egress rates throughout different treatments. (**B**) Effect of drug incubation on non-infected HFF. The graph presents a change on event number within the non-fluorescent HFF gate. Data represent the mean ±SEM of three independent experiments (except for DMSO treatment that has two independent experiment), six technical replicates on each. Significance was calculated using one-way Anova, Bonferroni's multiple comparisons P value ***< 0.001.

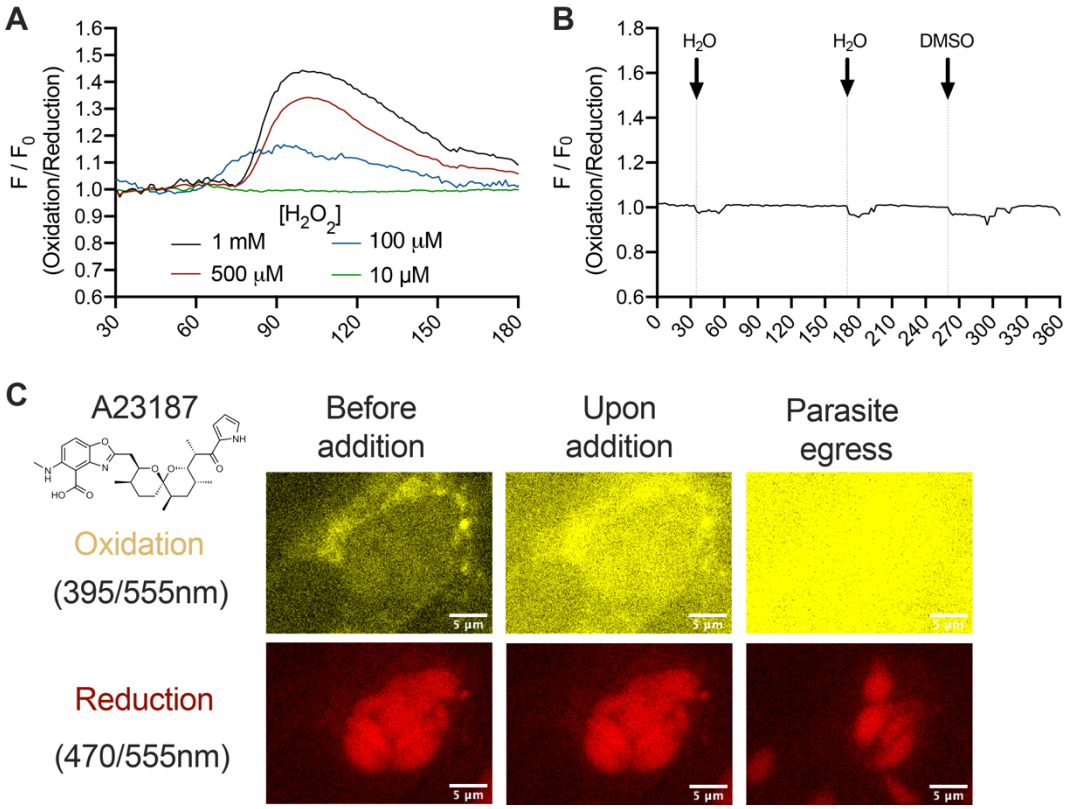

Figure supplement 3: Exploring the redox sensitivity of RH-GRX1-roGFP2 parasites to H_2O_2. (**A**) Tracking the GSH/GSSG change upon different concentration of H_2O_2. Among the concentration tested, 10 µM was the only one that did not induce a change in redox within the parasite cytosol. Data are representative of five infected vacuoles from each concentration, one independent experiment. (**B**) Water (vehicle control for H_2O_2) and DMSO (vehicle control for A23187) do not trigger change in GSH/GSSG. Data are representative of 12 vacuoles from three independent experiments. (**C**) Autofluorescence effect of A23187 drug on oxidation channel makes this ionophore unsuitable for ratiometric analyses of GRX1-roGFP2 sensor. Widefield microscope imaging depicting an egress induce by A23187. The structure of A23187 is shown.

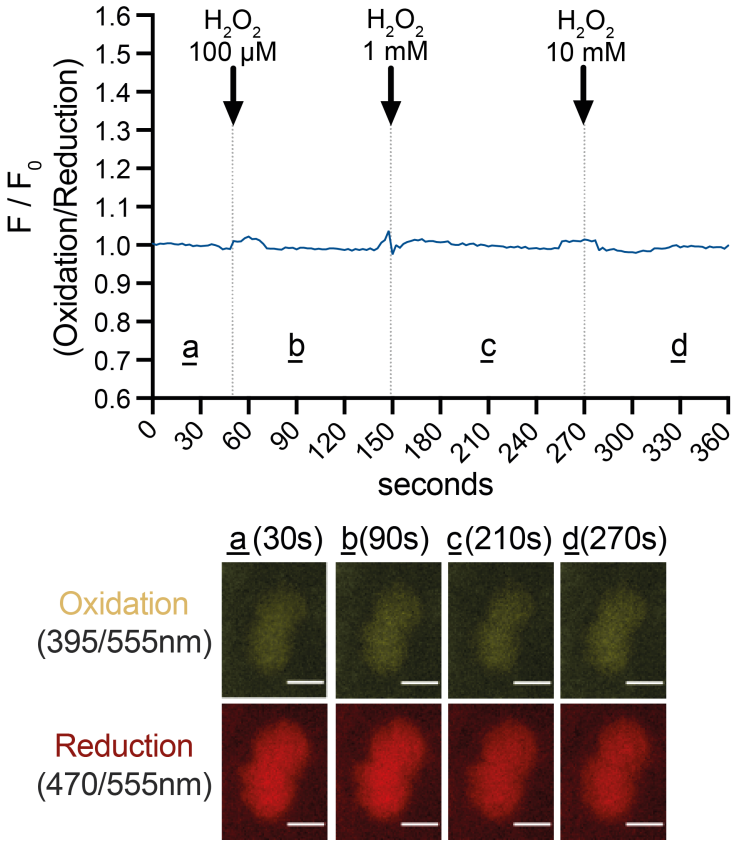

892
893

894 **Supplemental Figure 4:** Inactivation of the catalytic domain of glutaredoxin 1 makes the GRX1-
895 roGFP2 redox sensor insensitive to changes in GSH/GSSH. Parasite expressing GRX1ser-roGFP2 do
896 not display fluorescent changes in either channel (reduction or oxidation) upon addition of H_2O_2.
897 Data are representative of 12 infected vacuole, three independent experiments. Black arrows indicate
898 the time of H_2O_2 addition.
899

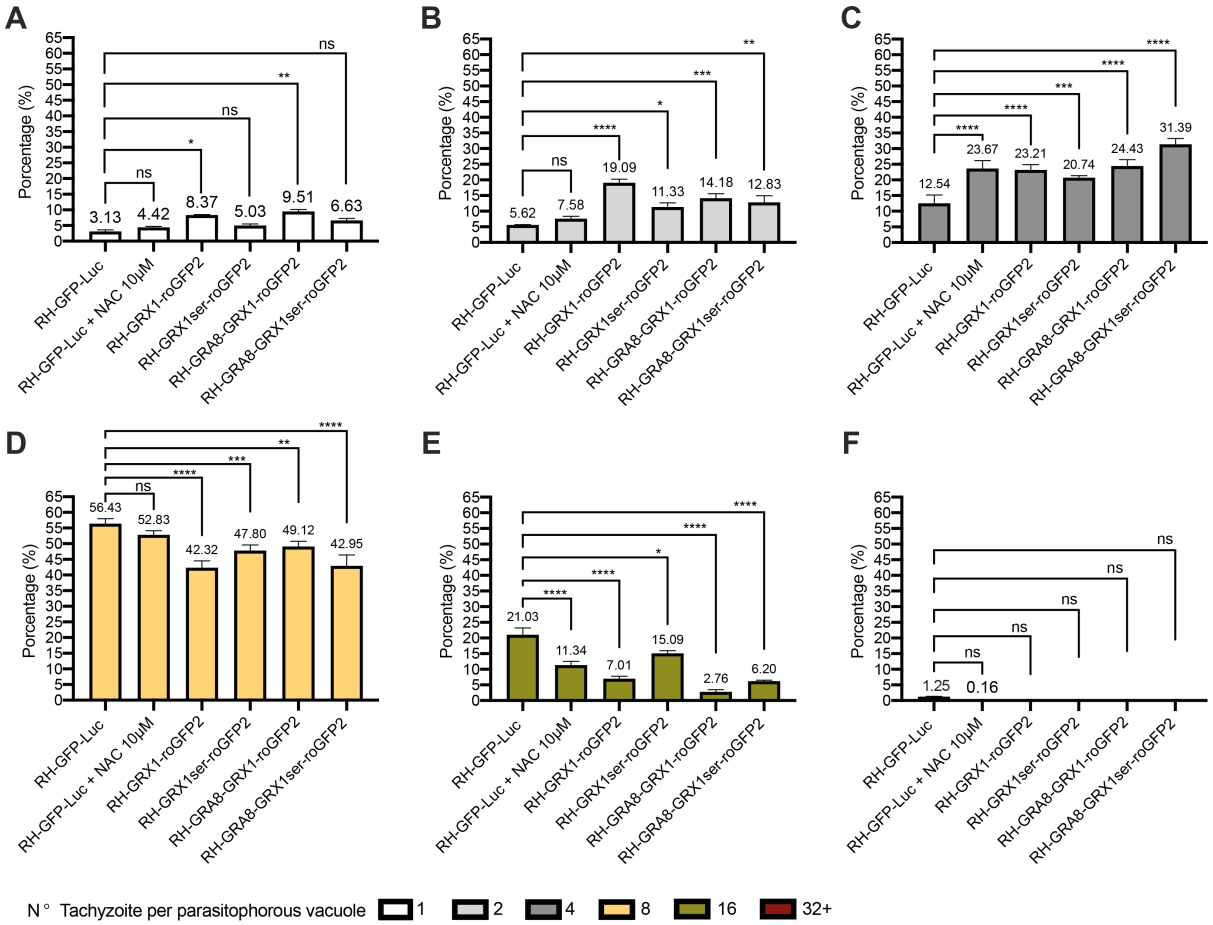

Figure supplement 5: Effect of redox sensors on *T. gondii* parasite growth. Each graph presents parasites/vacuole counts after 20 hours of intracellular growth. The mean values are displayed over each bar for three independent experiments. (**A**) Percentage (%) of vacuoles contain one parasite. (**B**) % of vacuoles with two parasites. (**C**) % of vacuoles with four parasites. (**D**) % of vacuoles with eight parasites. (**E**) % of vacuoles with 16 parasites. (**F**) % of vacuoles with more than 32 parasites. Significance was calculated using two-way Anova, Bonferroni's multiple comparisons test. P values: *< 0.05; **< 0.01, ***< 0.001 and ****< 0.0001.

Primer name	Primer number	Sequence (5'-3')
Fw-GRX1-roGFP2	1	ctcgttggcatttttttcttgatggctcaagagtttgtgaac
Rv-GRX1-roGFP2	2	agtgagcacaacggtgattattacttgtacagctcgtccatg
Fw-GRA8-GRX1-roGFP2	3	ctcgttggcatttttttcttgatggctttaccattgcgtgttt cggccacggtgttcgtggtcttcgctgtctttggtgtagct cgcgccatggggaaggtggttgtgttc
Fw-GRX1ser23-26	4	ccagcccaccagcccgtacagcag
Rv-GRX1ser23-26	5	atgaacacaaccaccttcccagg
Rv-GRA8-GRX1ser23-26	6	atgaacacaaccaccttccccat
Fw-pTUB8 sequence	7	cagaagacatccaccaaacg
Rv-pTUB8 sequence	8	gctgcgaaacactcctatttag
Fw-jRCaMP1b	9	actttcgtcgtagtcttaatctacttcgctgtcatcatttgtac
Rv-jRCaMP1b	10	tccaggaccaatgctgcagaacgagcttg
Fw-5'UTR of GRA1	11	tgctcaccatcttgcttgatttcttcaaag
Rv-5'UTR of GRA1	12	ccggactacgcgtagttaattcgaaggctgtagtactg
Fw-GFP-T2A-fusion	13	tctgcagcattggtcctggattttcttctacatc
Rv-GFP-T2A-fusion	14	atcaagcaagatggtgagcaagggcgag
Fw-HXGPRT cassette	15	caagaatccccactccaagcatgcaggcgcagctggagaatggcca gaggcaggcatc
Rv-HXGPRT cassette	16	caaccggctgcatgcacgacgaagacatgtgcacctaaagccgcggaa gatccgatcttg
Rv-pSAg1::CAS9-U6::sg1/2 CDPK3	17	aacttgacatccccatttac
Fw-pSag1::Cas9-U6::sg1 CDPK3	18	gacgccagcctcgaaaaggggttttagagctagaaatagc
Fw-pSag1::Cas9-U6::sg2 CDPK3	19	tcagtccgtagttgggacaggttttagagctagaaatagc
Fw-sg1CDPK3	20	gtaatacgactcactatagggcgaattgggtacccaagtaagc agaagcacgct
Rv-sg1CDPK3	21	gtaaaagcttatcgataccgtcgacctcgagaattaaccctc actaaagg
Fw-5'HXGPRT cassette at CDPK3 locus	22	ggagtcacgcctgagtttga
Rv-5'HXGPRT cassette at CDPK3 locus	23	ggcctacgtgacttgctgat
Fw-3'HXGPRT cassette at CDPK3 locus	24	cttcaatgggtttggacgcc
Rv-3'HXGPRT cassette at CDPK3 locus	25	gaacaaaaggggtcggtcat
Fw-CDPK3 locus absent check	26	gcgcgttctcaggatgttcgt
Rv-CDPK3 locus absent check	27	cagtgtatctgcaacaaccaga

Table supplement 2: List of primers used to generate plasmid and check sequence / integration in this study.

925 **Supplement references**

926 1. Zhang ZW, Li TT, Wang JL, Liang QL, Zhang HS, Sun LX, et al. Functional
927 Characterization of Two Thioredoxin Proteins of Toxoplasma gondii Using the CRISPR-Cas9 System.
928 Front Vet Sci. 2020;7:614759.
929 2. Sheiner L, Demerly JL, Poulsen N, Beatty WL, Lucas O, Behnke MS, et al. A systematic
930 screen to discover and analyze apicoplast proteins identifies a conserved and essential protein import
931 factor. PLoS Pathog. 2011;7(12):e1002392.
932 3. Xue J, Jiang W, Chen Y, Gong F, Wang M, Zeng P, et al. Thioredoxin reductase from
933 Toxoplasma gondii: an essential virulence effector with antioxidant function. FASEB J.
934 2017;31(10):4447-57.
935 4. Biddau M, Ovciarikova J, Sheiner L. Experimental Approaches for Examining Apicoplast
936 Biology. Methods Mol Biol. 2020;2071:221-43.
937 5. Moncada D, Arenas A, Acosta A, Molina D, Hernandez A, Cardona N, et al. Role of the 52
938 KDa thioredoxin protein disulfide isomerase of Toxoplasma gondii during infection to human cells.
939 Exp Parasitol. 2016;164:36-42.
940 6. Almeida F, Sardinha-Silva A, da Silva TA, Pessoni AM, Pinzan CF, Alegre-Maller AC, et al.
941 Toxoplasma gondii Chitinase Induces Macrophage Activation. PLoS One. 2015;10(12):e0144507.
942 7. Ding M, Kwok LY, Schluter D, Clayton C, Soldati D. The antioxidant systems in
943 Toxoplasma gondii and the role of cytosolic catalase in defence against oxidative injury. Mol
944 Microbiol. 2004;51(1):47-61.
945 8. Gretes MC, Poole LB, Karplus PA. Peroxiredoxins in parasites. Antioxid Redox Signal.
946 2012;17(4):608-33.
947 9. Mastud P, Patankar S. An ambiguous N-terminus drives the dual targeting of an antioxidant
948 protein Thioredoxin peroxidase (TgTPx1/2) to endosymbiotic organelles in Toxoplasma gondii. PeerJ.
949 2019;7:e7215.
950 10. Ding M, Clayton C, Soldati D. Toxoplasma gondii catalase: are there peroxisomes in
951 toxoplasma? J Cell Sci. 2000;113 (Pt 13):2409-19.

952 11. Kaasch AJ, Joiner KA. Targeting and subcellular localization of Toxoplasma gondii catalase.
953 Identification of peroxisomes in an apicomplexan parasite. J Biol Chem. 2000;275(2):1112-8.
954 12. Odberg-Ferragut C, Renault JP, Viscogliosi E, Toursel C, Briche I, Engels A, et al. Molecular
955 cloning, expression analysis and iron metal cofactor characterisation of a superoxide dismutase from
956 Toxoplasma gondii. Mol Biochem Parasitol. 2000;106(1):121-9.
957